Supporting Information

Biosynthesis of the tetrahydroxynaphthalene-derived meroterpenoid furaquinocin via reductive deamination and intramolecular hydroalkoxylation of an alkene

Tomohiro Noguchi,[1] Fan Zhao,[1] Yoshitaka Moriwaki,[1,2] Hideaki Yamamoto,[1] Kei Kudo,[1] Ryuhei Nagata,[1] Takeo Tomita,[1] Tohru Terada,[1,2] Kentaro Shimizu,[1,2] Makoto Nishiyama,[1,2] and Tomohisa Kuzuyama[1,2,*]

[1]Graduate School of Agricultural and Life Sciences and [2]Collaborative Research Institute for Innovative Microbiology, The University of Tokyo, 1-1-1 Yayoi, Bunkyo-ku, Tokyo 113-8657, JAPAN, *utkuz@g.ecc.u-tokyo.ac.jp

Experimental Section

General

Biochemicals and enzymes for genetic manipulation were purchased from TaKaRa Bio (Ohtsu, Japan), New England Biolabs Japan (Tokyo, Japan) and TOYOBO (Osaka, Japan). Eluent additives in liquid chromatography were purchased from Sigma- Aldrich (St. Louis, MO). Nitrite and L-Asp were purchased from Kanto Chemical Co., Inc. ^{15}N labeled L-Glu and nitrite were purchased from SHOKO SCIENCE. All other reagents were purchased from FUJIFILM Wako Pure Chemical Industries (Osaka, Japan), Kanto Chemicals (Tokyo, Japan), Tokyo Chemical Industry (Tokyo, Japan) and Nacalai Tesque (Kyoto, Japan) unless otherwise noted. Flaviolin, 8-AF, MMF, GPP, furaquinocin D, and naphterpin were prepared in our previous work[1,2]. Cells were disrupted using a Branson Sonifier 250 (Emerson Japan, Tokyo, Japan). HR-ESI-MS spectra were collected using a SCIEX Triple TOF 5600 system equipped with a UFLC Nexera system (Shimadzu, Kyoto, Japan) or a SCIEX triple TOF X500R system equipped with an UFLC Nexera system (Shimazu; Kyoto, Japan). For HPLC-UV/VIS analysis, X-LC (JASCO, Tokyo) system was used. For HPLC-UV/VIS-MS analysis, ACQUITY UPLC H-Class system/ACQUITY QDa (Waters, Tokyo) was used. DNA manipulation was performed according to the manufacturer's instructions. NMR spectra were obtained using a JEOL ECA-600.

Bacterial strains and vectors

Escherichia coli DH5α was used for plasmid cloning. *E. coli* BL21 (DE3) and B834(DE3) were used for expressing recombinant proteins. *Streptomyces albus* G153 was used as a heterologous host. The pT7Blue T-vector (Novagen) was used for cloning PCR products. pHis8[3] was used for protein expression. A *Streptomyces-E. coli* shuttle vector, pSE101,[4] was used for heterologous expression. *E. coli* BW25141/pKD46 was used for λ RED recombination. pWHM-fura2[5] was used for gene disruption and heterologous expression. pUC118 apr[6] was used for double crossover deletion of *nphH*.

Purification of recombinant proteins from *E. coli* BL21(DE3)

The pHis8 vector (Novagen, Darmstadt, Germany) pET-26b(+) (Novagen, for NphH) were used for plasmid construction. Each gene (*fur4,6,16,17,21,nphH*) was amplified using the respective primer sets shown in **Table S2**. These sequenced genes were digested with corresponding restriction endonucleases to clone into pHis8 or pET-26b(+) vector. Fur7 was cloned in our previous work.[2]

After transformation of *E. coli* BL21(DE3), each transformant was cultivated in 100 mL TB medium (tryptone 1.2%, yeast extract 2.4%, glycerol 0.56%, K_2HPO_4 1.25% and KH_2PO_4 0.23% supplemented with corresponding antibiotics) at 37°C until OD600 reaches 0.4-0.6. After cooling the culture on ice for 10 minutes, isopropyl β-D-thiogalactopyranoside (IPTG) was added to the culture at a final concentration of 100 μM to induce gene expression culture was further incubated at 18°C for 12 h. The cells were harvested by centrifugation at 4°C (5000 rpm, 10 min) and washed by 20 mL of Wash buffer (20 mM Tris-HCl pH 8.0, 500 mM NaCl, 20 mM imidazole-HCl pH 8.0, and 20% glycerol), followed by centrifugation at 4°C (5000 rpm, 10 min). The washed pellet was resuspended in Wash buffer again and lysed by sonication on ice. Cell debris was removed by centrifugation at 4°C (17,000 rpm, 20 min). Two mL slurry of Ni- NTA Superflow Resin (Qiagen, Tokyo, Japan) was added and incubated with the supernatant at 4 °C for 1 h. The resulting mixture was loaded on an Econo-Pac® chromatography column (Bio-Rad, Hercules, CA) and resins were washed with 40 mL of Wash buffer and then eluted with 10 mL of Elution buffer (20 mM Tris-HCl pH 8.0, 500 mM NaCl, 250 mM imidazole-HCl pH 8.0, and 20% glycerol). Each purified protein was examined by SDS-PAGE. Finally, the purified proteins were concentrated using Vivaspin® 20

ultrafiltration unit (Sartorius) and then aliquoted and stored at -80°C.

Purification of recombinant proteins from *S. albus* G153

The vector pSE101 was used for gene expression in *S. albus* G153 strain. The plasmid pSE101-*fur3*, pSE101-*fur5* and pSE101-*nphH* were constructed by subcloning corresponding DNA fragments into the *Hin*dIII and *Xba*I sites of pSE101. pSE101-*fur3* and pSE101-*fur5* were transformed into *S. albus* G153, using the polyethylene glycol-mediated protoplast transformation.[7] Each transformant was pre-cultivated in 10 mL of TSB medium with 30 μg/mL thiostrepton at 30°C, 300 rpm for 2 days. Two % of the seed culture was inoculated into 100 mL of YEME medium (10.3 g Sucrose, 0.3 g yeast extract, 0.5 g peptone, 1.0 g glucose, 0.3 g malt extract, separately autoclaved 0.5 mL 1 M $MgCl_2 \cdot 6H_2O$) or TSB medium with 30 μg/mL thiostrepton at 28°C for 3 days. Protein purification procedures are the same as those from *E. coli* BL21(DE3).

LC-HRMS analysis

The products of Fur5 or NphH reaction mixture, and the cultural broth of CL190WT, CL190Δ*nphH*, CL190Δ*nphH*+pSE101-*nphH* were analyzed by LC-electrospray ionization (ESI)-high-resolution mass spectrometry (HRMS) using a SCIEX Triple TOF 5600 system equipped with an Ultra-Fast Liquid Chromatograph (UFLC) Nexera system (Shimadzu; Kyoto, Japan). The UFLC system was equipped with a CAPCELLPAK C18 column (2.0 × 50 mm; Shiseido, Tokyo, Japan) and eluted at a flow rate of 0.4 mL/min. The mobile phase was composed of **A:** H_2O + 0.1% formic acid; mobile phase **B:** acetonitrile + 0.1% formic acid. A linear gradient of 10−90% **B** for 4 min, 90% **B** for 1 min, and 10% **B** for 5 min. MS and MS/MS parameters were as follows: acquisition mass range, *m/z* 50−1500; TOF accumulation time, 0.1 s; MS/MS accumulation time, 0.04 s; Collision Energy, 30 eV; Ion Source Gas 1, 50 psi; Ion Source Gas 2, 50 psi; Curtain gas, 25 psi; Ion spray voltage Floating, 5500 v; Temperature, 550 °C. MS data were analyzed with a PeakView software (SCIEX).

Derivatized 8-diazoflaviolin by Fur5 reaction or the cultural broth of *S. albus* G153/ pWFQΔ*fur4* and *S. albus* G153/ pWFQΔ*fur5* were analyzed by LC-electrospray ionization (ESI)-high-resolution mass spectrometry (HRMS) using a SCIEX triple TOF X500R system equipped with an UFLC Nexera system (Shimazu; Kyoto, Japan). The UFLC system was equipped with a CAPCELLPAK C18 IF column (2.0 mm × 50 mm; Shiseido, Tokyo, Japan) and eluted at a flow rate of 0.4 mL/min. The mobile phase was composed of **A:** H_2O + 0.1% formic acid; mobile phase **B:** acetonitrile. A linear gradient of 10−90% **B** for 4 min, 90% **B** for 1 min, and 10% **B** for 5 min.

LC-UV/VIS-MS analysis

The products of reaction mixtures of the Fur4, 5, 6, and 7 were analyzed by HPLC-UV/VIS-MS with the ACQUITY UPLC H-class system/ACQUITY QDa. The HPLC-UV/VIS-MS is equipped with a C18 column (ACQUITY UPLC BEH C18 2.1 × 50 mm, Waters) and eluted at a flow rate of 0.4 mL/min. LC conditions were as follows: mobile phase **A**, H_2O+0.1% Formic acid; mobile phase **B**, Acetonitrile+0.1% Formic acid; 0%–90% **B** over 4 min, 90% **B** for 1 min, and then 10% **B** for 5 min, at a flow rate of 0.4 mL/min. Multiple-wavelength monitoring was performed at 200−650 nm.

HPLC-UV/VIS analysis

ATP consumption analysis of Fur5 reaction mixture was monitored by the absorbance at 260 nm using a HPLC system equipped with a Capcell Pak C18 MGII column (4.6 φ × 250 mm; ambient temperature; Shiseido, Tokyo, Japan). LC conditions were as follows: mobile phase **A**, H_2O + 5 mM dibutylammonium acetate (DBAA); mobile phase **B**, methanol;

20−90% **B** over 20 min and 90-20% **B** over 1 min, followed by 20% **B** for 15 min, at a flow rate of 1 ml min^{-1}.

The products of Fur16,17 reaction mixture were analyzed using X-LC system equipped with a Shiseido CAPCELL PAK C18IF column (2.0 Φ x 50 mm; Shiseido, Tokyo). LC conditions were as follows: mobile phase **A**, H_2O+0.1% Formic acid; mobile phase B, Acetonitrile+0.1% Formic acid; 0%–90% **B** over 4 min, 50% **B** for 1 min and then 10% **B** for 5 min, at a flow rate of 0.4 mL/min. After 1 hour at 30°C, the reaction was stopped by adding an equal volume of MeOH to the reaction solution. The precipitate was removed by centrifugation, and an equal volume of 10 mg/mL Griess-Romijn reagent was added to the centrifuged supernatant and analyzed by X-LC. The detection of nitrite with Griess-Romijn reagent involves the conversion of nitrite to azo compounds by reaction with the amino group of sulfanilamide under acidic conditions, followed by azo coupling with *N*-1-napthylethylenediamine dihydrochloride (NED), resulting in detection at 528 nm absorbance.

GC-MS analysis

GC-MS analysis was performed using a GCMS-QP2020 system equipped with a Msieve-5A, (30 m, 0.32 mm ID, 30 µm film) (Restek, Pennsylvania, USA). Injector temperature: 200 °C, temperature program: 40 °C constant.

In vitro assay for the Fur16 and Fur17 reaction.

The standard reaction was performed at 30 °C for 1h in 100 µL reaction mixture containing 100 mM HEPES-NaOH, pH 7.5, 1 mM NADH/NADPH, 1 mM L-Asp, 1 mM DTT, 14 µM Fur16, and 19 µM Fur17. After incubation, the reaction was quenched by adding 100 µL of methanol. After centrifugation, the supernatant was subjected to LC-UV/VIS-MS analysis.

In vitro assay for the Fur5 reaction.

The standard reaction was performed at 30 °C for 1h in 100 µL reaction mixture containing 100 mM HEPES-NaOH, pH 7.5, 100 µM 8-AF, 1 mM ATP, 5 mM $MgCl_2$, 1 mM $NaNO_2$ (or ^{15}N labeled one) and 2 µM Fur5. After incubation, the reaction was quenched by adding 100 µL of methanol. After centrifugation, the supernatant was subjected to LC-HRMS analysis or LC-UV/VIS-MS analysis.

The reaction condition for the ATP detection was performed at 30 °C for 2h in 100 µL reaction mixture containing 100 mM HEPES-NaOH, pH 7.5, 200µM 8-AF, 200 µM ATP, 1 mM $MgCl_2$, 1 mM $NaNO_2$, and 4 µM Fur5. After centrifugation, the supernatant was subjected to HPLC-UV/VIS analysis.

For ^1H NMR analysis, the large-scale reaction was performed at 4°C for 4 days in 160 mL reaction mixture containing 100 mM HEPES-NaOH, pH 7.5, 4.1 mg 8-AF, 5 mM ATP, 10 mM $MgCl_2$, 5 mM $NaNO_2$, and Fur5 from 8 L culture of *S. albus* G153/pSE101-*fur5*. Derivatization by Ethyl 2-methylacetoacetate, which was previously used to detect a diazo group[8] was performed at 4 °C for 9 days. The product was extracted three times with an equivalent volume of ethyl acetate and dried under reduced pressure in an evaporator. The mobile phase of TLC was chloroform:MeOH = 20:1 with 0.1% formic acid. The fraction of R_f = 0.33 was scraped off, dissolved in methanol, and further purified by preparative HPLC using 50% acetonitrile with 0.1% formic acid as the mobile phase. A very small amount of derivatized 8-diazoflaviolin was obtained by preparative HPLC using 50% acetonitrile with 0.1% formic acid as the mobile phase. Derivatized 8-diazoflaviolin dissolved in CD_3OD was subjected to ^1H NMR analysis. An equal volume of mobile phase (50% acetonitrile with 0.1% formic acid) was collected when derivatized **5** was fractionated and the solvent was evaporated to prepare the NMR sample of the blank fraction.

In vitro assay for the NphH reaction.

The standard reaction was performed at 30 °C for 1h in 100 μL reaction mixture containing 100 mM HEPES-NaOH, pH 7.5, 100 μM 8-AF, 1 mM ATP, 5 mM $MgCl_2$, 1 mM $NaNO_2$, 10% (v/v) glycerol and 10 μM Fur5 or NphH. After incubation, the reaction was quenched by adding 100 μL of methanol. After centrifugation, the supernatant was subjected to LC-HRMS analysis.

In vitro assay for the Fur6 reaction.

The standard reaction was performed at 30 °C for 1h in 100 μL reaction mixture containing 100 mM HEPES-NaOH, pH 7.5, 100 μM flaviolin, 1 mM SAM, 5 mM dithionite or NADPH, and 2 μM Fur6. After centrifugation, the supernatant was subjected to LC-UV/VIS-MS analysis.

In vitro assay for the Fur5 and Fur6 reaction.

The standard reaction was performed at 30 °C for 1h in 100 μL reaction mixture containing 100 mM HEPES-NaOH, pH 7.5, 100 μM 8-AF, 1 mM ATP, 5 mM $MgCl_2$, 1 mM $NaNO_2$, 1 mM SAM, 1 mM NADPH, 2 μM Fur5, and 2 μM Fur6. After centrifugation, the supernatant was subjected to LC-UV/VIS-MS analysis.

The sequential reaction was performed at 30 °C for 1h in 100 μL reaction mixture under the conditions of Reaction Mixture 1 (100 mM HEPES-NaOH, pH 7.5, 100 μM 8-AF, 1 mM ATP, 5 mM $MgCl_2$, 1 mM $NaNO_2$, and 2 μM Fur5), followed by ultrafiltration (removal of proteins larger than 10 kDa), and then the reaction was performed under the conditions of Reaction Mixture 2 (1 mM SAM, 1 mM NADPH, and 2 μM Fur6).

The reaction with a wide range of reducing agents was performed at 30 °C for 1h in 100 μL reaction mixture containing 100 mM HEPES-NaOH, pH 7.5, 100 μM 8-AF, 1 mM ATP, 5 mM $MgCl_2$, 1 mM $NaNO_2$, 1 mM SAM, 1 mM reducing agents, 2 μM Fur5, and 2 μM Fur6. After centrifugation, the supernatant was subjected to LC-HRMS analysis.

The reaction condition for the N_2 gas detection was performed at 30 °C for 2h in 100 μL reaction mixture containing 100 mM HEPES-NaOH, pH 7.5, 200 μM 8-AF, 1 mM ATP, 5 mM $MgCl_2$, 1 mM $NaNO_2$ (or ^{15}N labeled one), 1 mM SAM, 1 mM NADPH, 2 μM Fur5, and 2 μM Fur6. After centrifugation, the supernatant was subjected to LC-UV/VIS-MS analysis.

In vitro assay for the Fur3 reaction and ^{15}N 8-AF purification.

Fur3 reaction was performed at 30 °C for 6 days in a 50 mL reaction mixture containing 100 mM HEPES-NaOH, pH 7.5, 4 mg mompain, 1 mM L-Glu, 50 μM PLP, and 60 μM Fur3. After incubation, the reaction mixture was adsorbed on Sep-Pak C18 6 cc Vac Cartridge (Waters, 1 g Sorbent per Cartridge, 55-105 μm, 30/pk), washed with miliQ (+0.1% TFA), 20% MeOH (0.1% TFA), and eluted with 100% MeOH (+0.1% TFA). The eluted fractions were dried, and the residue was purified by preparative HPLC using 25% acetonitrile as the mobile phase.

In vitro assay for the Fur4 reaction.

The standard reaction was performed at 30 °C for 1h in 100 μL reaction mixture containing 100 mM HEPES-NaOH, pH 7.5, 100 μM 3-MF, 1 mM SAM, 5 mM dithionite, and 2 μM Fur4. After centrifugation, the supernatant was subjected to LC-UV/VIS-MS analysis.

In vitro assay for the Fur7 reaction.

The standard reaction was performed at 30 °C for 1h in 100 μL reaction mixture containing 100 mM HEPES-NaOH, pH 7.5, 100 μM MMF, 1 mM GPP, 5 mM dithionite, and 2 μM Fur7. After centrifugation, the supernatant was subjected to LC-UV/VIS-MS analysis.

In vitro assay for the Fur21 reaction.

The standard reaction was performed at 30 °C for 1h in 100 µL reaction mixture containing 100 mM HEPES-NaOH, pH 7.5, 100 µM Fur-P1, 1 mM SAM, 5 mM dithionite, and 2 µM Fur21. After centrifugation, the supernatant was subjected to LC-UV/VIS-MS analysis.

Purification of Fur6 for crystallization

E. coli strain BL21(DE3) cells were transformed with the pHis8-*fur6* and cultured as described earlier. The cells transformed with the pHis8-*fur6* were suspended in the wash buffer described above that comprised 50 mM Tris-HCl pH 8.0, 150 mM NaCl, 10% (v/v) glycerol, and 20 mM imidazole and disrupted by sonication. The sonicate was centrifuged at 34,000 × g for 20 min at 4°C. The supernatants were loaded onto a Ni-NTA agarose column (QIAGEN) pre-equilibrated with the wash buffer. After washing with the wash buffer, the proteins were eluted with the elution buffer described above containing 250 mM imidazole. The collected samples were concentrated to 1 mL by centrifuging using an Amicon Ultra-15 10 K centrifugal filter (Merck, Darmstadt, Germany). The concentrated Fur6 was loaded onto a HiLoad 16/600 Superdex 200 size-exclusion chromatography column (Cytiva, Tokyo, Japan) pre-equilibrated with the equilibration buffer (20 mM Tris-HCl pH 8.0, 150 mM NaCl). Fur6 was eluted as a single peak of monomer size (approximately 38 kDa). The fractions abundant in the purified Fur6 were collected and substituted by changing buffers for the crystallization buffer that comprised of 20 mM Tris-HCl pH 8.0, 150 mM NaCl. Finally, the purified proteins were concentrated by centrifugation using an Amicon Ultra-15 30 K centrifugal filter (Merck), frozen in liquid nitrogen, and stored at –80°C until use.

Selenomethionine (SeMet)-substituted Fur6 was prepared in the same way as the native Fur6, except that cells expressing Fur6 were cultured in the medium containing SeMet as follows. *E. coli* strain B834(DE3) cells were transformed with the pHis8-fur6, and were pre-cultured in 5 mL of LB medium containing 50 µg/mL kanamycin overnight at 37°C. After the induction with isopropyl β-thiogalactopyranoside, the cells were grown at 18 °C for 16 h in 1.6 L of SeMet core medium (Wako) supplemented with 16 g of glucose, 400 mg of $MgSO_4 \cdot 7H_2O$, 6.7 mg of $FeSO_4 \cdot 7H_2O$, 16 ml of vitamin growth supplement (Sigma-Aldrich), 50 µg mL^{-1} of kanamycin, and 40 mg of seleno-L-methionine (Wako). The *E. coli* cells were harvested, washed, and suspended in the wash buffer. SeMet-substituted Fur6 protein was purified in the same way as native Fur6.

Crystallization conditions were screened by the hanging-drop vapor-diffusion method using Crystal Screen (Hampton Research), the Wizard crystallization screen series (Emerald Bio), and PEG/Ion Screen (Hampton Research) at 20°C. The screens were set up using 2.0 µL drops consisting of 1.0 µL reservoir solution and 1.0 µL 10 mg ml^{-1} Fur6 solution with and without 2 mM *S*-adenosyl homocysteine. Crystals of Fur6 in complex with *S*-adenosyl homocysteine were obtained in the droplet using a solution containing 20% w/v Polyethylene glycol 3,350 and 0.2 M Calcium acetate hydrate pH7.5 (PEG/Ion Screen #28). Crystals of SeMet-substituted Fur6 were obtained from droplets of essentially the same conditions used for unsubstituted Fur6.

Data collection, structure determination, and refinement of Fur6

Prior to data collection from SeMet-Fur6, the crystals were briefly soaked in a cryo-protectant solution supplemented with 30% (v/v) PEG 3350, then flash-cooled in a nitrogen-gas stream at 95 K. The X-ray diffraction experiments were performed at the SPring-8 beamlines BL32XU (Hyogo, Japan) or Photon Factory, High Energy Accelerator Research Organization (KEK, Tsukuba, Japan). SeMet single wavelength anomalous diffraction (Se-SAD) data were collected at the BL-5A station of KEK. Diffraction images were indexed, integrated, and scaled using the XDS package[9] from CCP4 suite. The data collection statistics are shown in Table S3. Structure determination via the SAD method was performed using an automated pipeline for structure determination, Crank2.[10] The data from crystals

of native Fur6 in complex with *S*-adenosyl homocysteine collected at a wavelength of 1.0 Å were used for subsequent molecular replacement and crystallographic refinement. Molecular replacement was performed by Phaser[11] in the CCP4 program suite.[12] Model correction into the electron density map was performed using Coot,[13] and the real space refinement was performed using Refmac 5.5. [14] Ramachandran plots produced by the program Molprobity[15] are summarized in Table S3. The figures were prepared using PyMOL (https://pymol.org/2/). The atomic coordinates have been deposited in the RCSB PDB with the accession number 8HAR.

pK_a calculation

The pK_a values of all hydroxy groups of PHN were calculated with a software program Epik (Release 2021-1)[16,17] using the optimized geometry obtained by Gaussian 16 Rev B.01. Default parameters were used throughout the calculations.

Molecular dynamics (MD) simulations

The crystal structure of Fur6 in complex with SAH was used to construct model structures of the Fur6-SAM-PHN ternary complex. Since Fur6 forms a dimer structure, MD simulations were performed for dimeric forms. Hydrogen atoms were added to the protein and all histidine residues were protonated at the Nε2 atom. The geometries of SAM and PHN were optimized at the B3LYP/6-31G(d) level and their partial charges were obtained by the restrained electrostatic potential (RESP) method using the electrostatic potentials calculated at the HF/6-31G(d) level for the optimized geometries with Gaussian 16 Rev B.01.[18] The ANTECHAMBER module[19] was used to parameterize the cofactor and the substrate. The ff14SB force field[20] and the general AMBER force field 2 (GAFF2)[21] were used for the protein and organic molecules, respectively. For the MD simulations, the initial coordinates of the methyl group of SAM were generated by the LEaP module[22] using the optimized SAM geometry as a template.

The prepared complex structure was fully solvated with the TIP3P explicit water model[23] in a cubic periodic box with an edge length of 120 Å using the AMBER LEaP module. Na^+ and Cl^- ions were added at a concentration of 0.15 M to neutralize the system. The system was first relaxed using 200 steps of steepest descent minimization with 1,000 kcal mol^{-1} $Å^{-2}$ position restraints applied to the non-hydrogen atoms of the protein. Subsequently, the restraints were removed, and the entire system was subjected to 200 steps of steepest descent minimization. Next, MD simulations were performed for 1 ns under the *NPT* ensemble to gradually heat and equilibrate the system at 300 K. In this equilibration run, distance restraints were imposed on atom pairs that form hydrogen bonds in the active site (Table S4). After the equilibration, 50-ns conventional production runs were performed. Van der Waals interactions were calculated with a cut-off radius of 10 Å. The particle mesh Ewald (PME) method[24] was used to calculate electrostatic interactions. The SHAKE algorithm[25] was used to constrain the bonds including hydrogen atoms. The integration time step was set to 2 fs. The Berendsen weak coupling algorithm[26] was used to maintain a constant temperature and pressure. All the energy minimization, equilibration, and production runs were performed using the PMEMD module of AMBER 20.[27]

Gene disruption and heterologous expression analysis of pWFQ

For the construction of the *fur4* disruption plasmid, *fur4* gene located on pWFQ was replaced by the *aph* cassette via λRED recombination. The linear DNA fragment containing *aph* gene was amplified by PCR with pKU479[28] as a template using two primer pairs, fur4_loxP_f and fur4_loxP_r. The amplified fragment was introduced into *E. coli* BW25141/pKD46/pWFQ to yield pWFQΔfur4.[29] The fur deleted construct, pWFQΔ*fur4*, was introduced into *S. albus*

G153, and the resultant transformant, *S. albus* G153/pWFQΔ*fur4* was used for the further analysis.

Transformants of S. albus G153/ pWFQ*Δfur4* were pre-cultured in TSB (+30 μg/mL tsr) medium at 30°C for 2 days. The pre-culture was inoculated 2% into 100 mL of NMMP (+30 μg/mL tsr) medium and incubated at 27°C for 5 days. Equal volumes of methanol were added to the culture medium, and the centrifugal supernatant was subjected to LC-HRMS analysis.

S. albus G153/pWFQΔ*fur5* was prepared by the same method as *S. albus* G153/pWFQΔ*fur4*.

Transformants of S. albus G153/ pWFQ*Δfur5* were pre-cultured in TSB (+30 μg/mL tsr) medium at 30°C for 2 days. The pre-culture was inoculated 2% into 100 mL of A1 (+30 μg/mL tsr) medium and incubated at 27°C for 4 days. Equal volumes of methanol were added to the culture medium, and the centrifugal supernatant was subjected to LC-HRMS analysis.

nphH disruption and cultural analysis of *Streptomyces* sp. CL190

Using primers dnphH_up_f and dnphH_up_r for amplifying the upstream 2 kb region of nphH, and dnphH_down_f and dnphH_down_r for amplifying the downstream 2 kb region (Table 2-1), DNA fragments were amplified by PCR and cloned into the HindIII site of pUC118apr to construct the gene disruption plasmid pUC118apr*ΔnphH*. The resulting plasmid was transformed into *Streptomyces* sp. CL190, and apramycin-resistant colonies were selected to obtain single-crossover mutants.

The single-crossover mutants were cultured on R2YE medium at 30°C for 2 days, followed by protoplast formation. After appropriate dilution, cultures were spread onto R2YE agar medium to obtain single colonies. These single colonies were subsequently streaked onto both TSB agar and TSB agar containing 25 μg ml^{-1} apramycin. Colonies that showed sensitivity to apramycin were selected as *Streptomyces* sp. CL190*ΔnphH* mutants, referred to hereafter as CL190*ΔnphH*. Gene disruption in the selected strains was confirmed by colony PCR using the verification primers dnphH_check_f and dnphH_check_r, as listed in Table S2. The plasmid pSE101-nphH for *nphH* complementation was constructed by amplifying a DNA fragment from the CL190 genome template using the primers pSE101_nphH_f and pSE101_nphH_r. The amplified fragment was then cloned into the HindIII and XbaI sites of pSE101. The resulting pSE101-nphH plasmid was transformed into the CL190Δ*nphH* mutant to obtain the complementation strain, CL190Δ*nphH*+pSE101-nphH.

CL190WT, CL190*ΔnphH*, CL190*ΔnphH*+pSE101-*nphH* were pre-cultured in TSB medium at 30°C for 2 days. The pre-culture was inoculated 2% into 100 mL of KG medium and incubated at 27°C for 1-3 days. Equal volumes of methanol were added to the culture medium, and the centrifugal supernatant was subjected to LC-HRMS analysis.

Supplementary Tables

Table S1 Annotation of each protein encoded by the *fur* cluster.

Gene Product	Amino acids (no.)	Proposed function	Sequence similarity (protein, origin)	Similarity / Identity (%)	Protein accession number
Fur1	356	Type III polyketide synthase	RppA, *Streptomyces antibioticus*	95/91	BAB91443
Fur2	188	Quinone forming monooxygenase	MomA, *Streptomyces antibioticus*	87/81	BAD89290
Fur3	385	PLP dependent aminotransferase	NphE, *Streptomyces* sp. CL190	88/80	BAM67036
Fur4	331	SAM dependent O-methyltransferase	Fnq9, *Streptomyces cinnamonensis*	88/77	CAL34087
Fur5	528	fatty-acid-CoA ligase	NapB4, *Streptomyces* sp. CNQ525	85/74	ABS50451
Fu6	357	SAM dependent C-methyltransferase	Fnq27, *Streptomyces cinnamonensis*	87/78	CAL34105
Fur7	307	prenyltransferase	Fnq26, *Streptomyces cinnamonensis*	81/66	CAL34104
Fur8	434	cytochrome P450	cytochrome P450, C-methyltransferase	50/33	ZP_10449418
Fur15	324	Acetoacetyl CoA synthase	NphT7, *Streptomyces* sp. CL190	81/73	D7URV0
Fur16	652	*N*-monooxygenase	CreE, *Streptomyces cremeus*	69/59	CAL34098
Fur17	484	Nitrosuccinate lyase	CreD, *Streptomyces cremeus*	67/59	CAL34099
Fur18	209	hypothetical protein	NapU1, *Streptomyces* sp. CNQ525	64/46	ABS50476
Fur19	352	GPP synthase	Fnq23, *Streptomyces cinnamonensis*	80/71	CAL34101
Fur20	282	undecaprenyl diphosphate synthase	*Streptomyces davawensis* JCM 4913	97/91	CCK32344
Fur21	398	SAM dependent C-methyltransferase	Fnq27, *Streptomyces cinnamonensis*	75/60	CAL34105

The nucleotide sequence of the *fur* cluster is deposited in the DDBJ/EMBL/GenBank nucleotide sequence database under the accession number AB212624.

Table S2 List of primers used in this study.

Primer	Oligonucleotide sequence (5' to 3')
Fur3_fw	5'-GGGAAGCTTGACGCCCGGCCGCGAACCGCACGC-3'
Fur3_rv	5'-GGGTCTAGACTCAGTGGTGGTGGTGGTGGTGGTGTGCTGCCCCTCCTGGGCTCGG-3'
Fur4_fw	5'-GGGCCATGGCACGGACCACCAGCCGACTCCGGAC-3'
Fur4_rv	3'-GGGGGATCCTCACCGGGCGATGACCAGGGTGG-3'
HindIII_Fur5_fw_C	5'-GGGAAGCTTAGCAACGGAGGTACGGACATGAACGGCTCAGTGGCCTATCGCACG-3'
XbaI_Fur5_rvC10	5'-GGGTCTAGACTCAGTGGTGGTGGTGGTGGTGGTGGTGGTGCTCCCGGCCCTTGCGCTTGTC-3'
Fur6_fw	5'-GGGCCATGGCACGTCTGACCAGCCGGCCGC-3'
Fur6_rv	3'-GGGGGATCCTCACACGACCTTGGTCGCGG-3'
NcoI_Fur16_f	5'-GGGCCATGGCACCACCCGTCACTGCACCGTTG-3'
BamHI_Fur16_r	5'-GGGGGATCCTCACTGCGCGTAGGTCAGACCACG-3'
Fur17-fw	5'-GGGCCATGGCCCCAATGACACCAGCCTCACC-3'
Fur17-rv	5'-GGGGGATCCTCACGCAGATCGTGATGCAACG-3'
Fur21-fw	5'-GGGGGATCCTCCAACCCCGAAGCCGTACTCG-3'
Fur21-rv	5'-GGGAAGCTTTCAGTCCCGCTTCGTCGCGC-3'
fur4_loxP_f	5'-GGGCCACCGGCGTCGTCGGCGCCGCGGCCGCCCACTCGCTGTTCACCCACATGCAGTGAATTCGAGCGACTCGAGT-3'
fur4_loxP_r	5'-AAACCGGCCTTGACCAGCCAGTTGTGGTAGTCGGAGCGCCGCCAGGTGCCTCAGGGTACCGAGCGAACGCGTT-3'
fur5_loxP_f	5'-GCCTGCTCCCGGCCATGGCCGCGGCCGTCGACGAGACGACGCCCATCACCATGCAGTGAATTCGAGCGACTCGAGT-3'
fur5_loxP_r	5'-ACCTTGAGGGTGCCGGTGCGCGGCAGTTCGGCCTCGGGGATCTGGACCGGTCAGGGTACCGAGCGAACGCGTT-3'
d_fur4_check_f	5'-GACACGGCACCTTCGCGACCCACATCC-3'
d_fur4_check_r	5'GGAGCAGGCCTATGTGCAGTCCGCGTTTC3'
d_fur5_check_f	5'-GGGCTGTACTCCCACATCGCCCACCAGGAGG-3'
d_fur5_check_r	5'-GGGCGAAGCCCTCCTTGACCAGGAGGAGAAGC-3'
NphH_fw	5'-GGGCATATGAAGGGCTCTGTGGCCTACCAATCGATACAGAAG-3'
NphH_rv	5'-GGGCTCGAGGCCGCGGCTCTTGAGCTGGTCC-3'
dnphH_up_f	5'-GGGAAGCTTCCTGGGAGGGGCGGCATGACGAAC-3'
dnphH_up_r	5'-GGGTCTAGAGATCGGCGTCGACGGGTTCACGGC-3'
dnphH_down_f	5'-GGGTCTAGACAGATCCCCGAGGCCGAACTGCCG-3'
dnphH_down_r	5'-GGGAAGCTTCAGGTCGGCGAGCGCCTGCTCAAG-3'
dnphH_check_f	5'-GGGGAGACGGGCAACCCGTACGGCACC-3'
dnphH_check_r	5'-GGGCAGGGTCTCCACAGCGACACGCGAC-3'
pSE101_nphH_f	5'-GGGAAGCTTATGAAGGGCTCTGTGGCCTACCAATCGATACAG-3'
pSE101_nphH_r	5'-GGGTCTAGAGTCAGCCGCGGCTCTTGAGCTGGTC-3'

Table S3 X-ray data collection and refinement statistics.

		SeMet Fur6	Fur6
PDB code			8HAR
Data Collection			
Beamline		PF-NE3A	SPring-8 BL32XU
Wavelength (Å)		0.97876	1
Space group		P212121	P212121
Cell dimensions			
	a, b, c (Å)	72.53, 88.11, 120.82	74.98, 91.84, 125.35
	α, β, γ (°)	90, 90, 90	90, 90, 90
	Resolution (Å)[a]	2.18 (2.25-2.18)	2.12 (2.18-2.12)
	R_{merge} (%)[a,b]	10.6 (85.6)	
	R_{pim} (%)[a,b]	6.7 (55.9)	
	R_{sym} (%)[a]		26.4 (68.7)
	I/ σ (I)	11.6 (2.4)	5.93 (2.05)
	Completeness (%)	99.9 (100.0)	99.9 (99.7)
	No. of obs. reflections	262991	763438
	No. of uniq. reflections	41119	94785
	Redundancy	6.4	8.1
	$CC_{1/2}$ (%)[a]	99.7 (67.3)	98.4 (81.3)
Phasing			
	No. of Se sites	25	
	FOM[c]	0.20 (0.53)	
Refinement			
	Resolution (Å)		50-2.12
	R_{work}/R_{free} (%)		21.1/25.6
	No. of protein atoms		5303
	No. of Ligand/ion atoms		60
	No. of water molecules		120
	Averaged B-factor (Å^2)		
	Protein		41.5
	Ligand/ion		41.0
	Water		37.4
	R.m.s.d from ideal values		
	Bond length (Å)		0.004
	Bond angles (deg.)		1.3
	Ramachandran plot (%)		
	Favored		97.75
	Allowed		2.25
	Outliers		0

[a]Values in parentheses are for highest-resolution shell.

[b]$R_{merge}= \Sigma | I_i - \langle I \rangle | / \Sigma \langle I \rangle$.

[c]Figure of merit was calculated with the program Crank2

Table S4 The sets of distance restraints used in MD simulation models.

Atom 1	Atom 2	Equilibration distance r (Å)	Force constants k (kcal mol^{-1} Å^{-2})
Tyr137-OH	PHN359-O2	3.20	2.0
SAM358-OXT	Thr158-HG1	3.20	2.0
Arg147-NH1	Ala141-O	3.20	2.0
Arg147-NH1	Glu209-O	3.20	2.0
Arg147-NH2	Glu209-O	3.20	2.0
Arg147-NH2	Glu213-OE1	3.20	2.0
Met154-SD	PHN359-C6	4.20	2.0
Trp150-HE1	PHN359-O3	3.20	2.0
Ala181-O	SAM358-N	3.20	2.0

Supplementary Figures

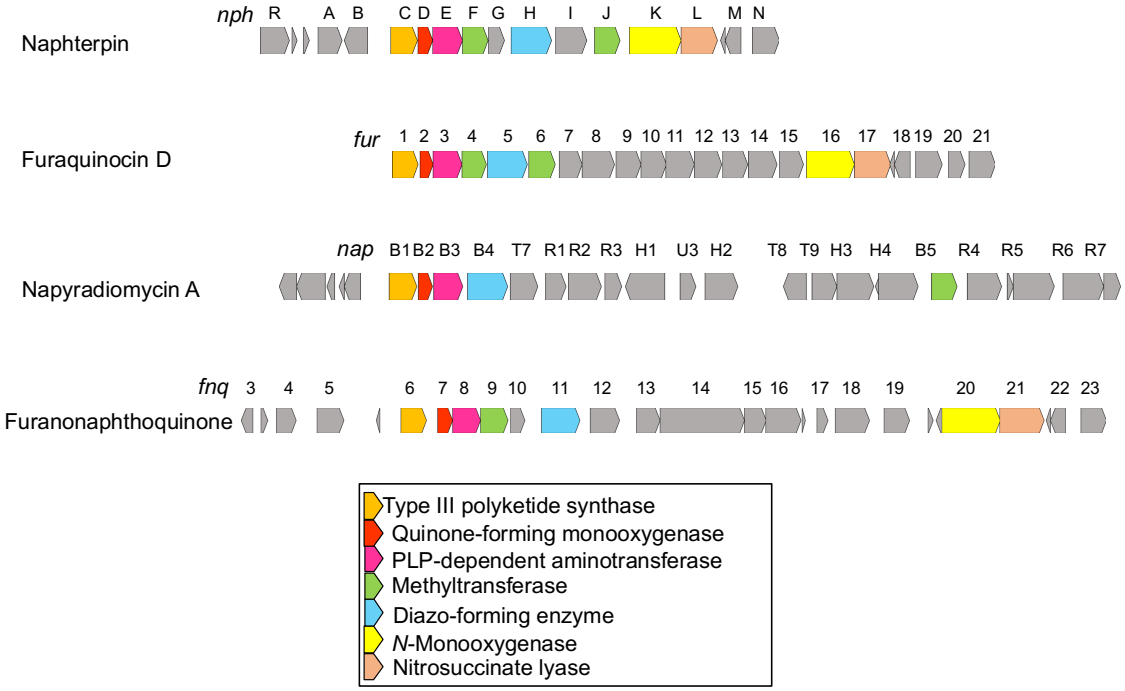

Figure S1. A conserved cassette among the biosynthetic cluster of meroterpenoids.

In addition to three contiguous *fur1-3* involved in the synthesis of 8-AF (**3**), nitrite-forming *fur16* and *fur17* homologs, diazo-forming *fur5* homologs, and methyltransferases are also conserved among the biosynthetic gene clusters for meroterpenoids such as naphterpin and furanonaphthoquinone

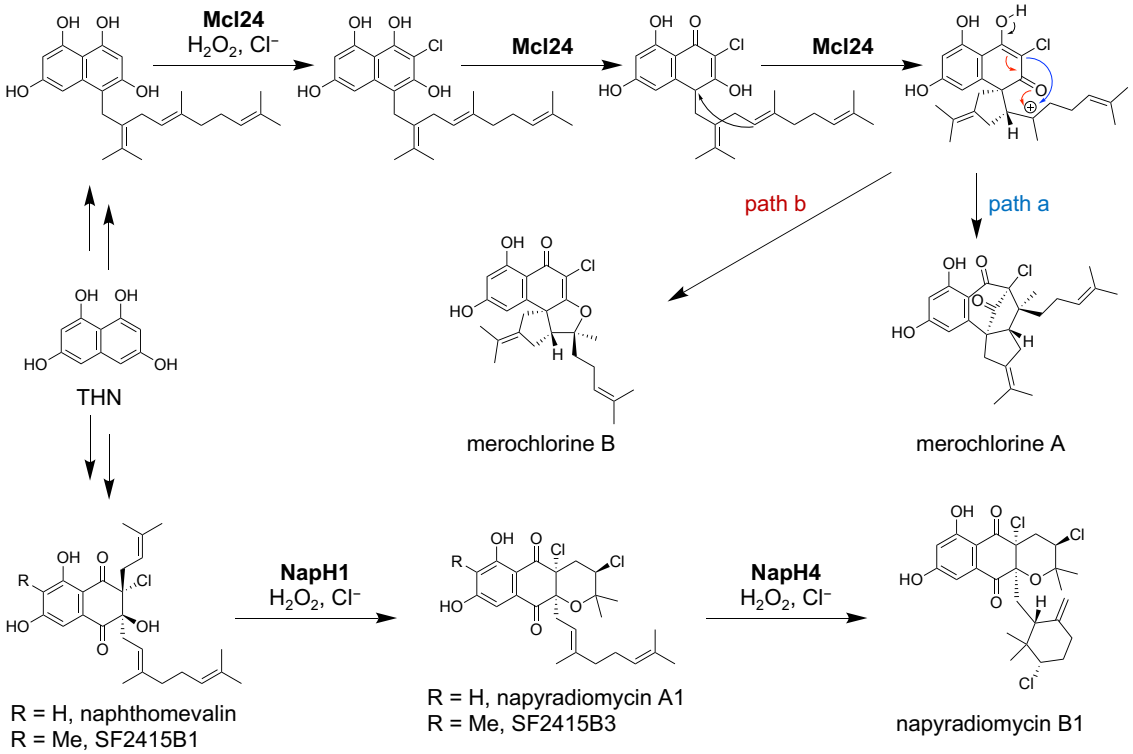

Figure S2. Cyclization by VHPOs in meroterpenoid biosynthesis.

Two vanadium-dependent haloperoxidase enzymes, NapH1 and NapH3, are involved in the biosynthesis of napyradiomycin. NapH1 catalyzes the initial halogenation and cyclization of the C-2 prenyl side chain to form the tricyclic 6,6,6 ring system, while NapH3 contributes to further modifications, such as additional chlorination or oxidative rearrangements. In the biosynthesis of merochlorin, the vanadium-dependent haloperoxidase Mcl24 catalyzes the C-2 monochlorination, oxidative dearomatization, and cyclization of the pre-merochlorin intermediate, constructing its unique bicyclo[3.2.1]octane structure. NapH3 is not directly involved in the merochlorin pathway.

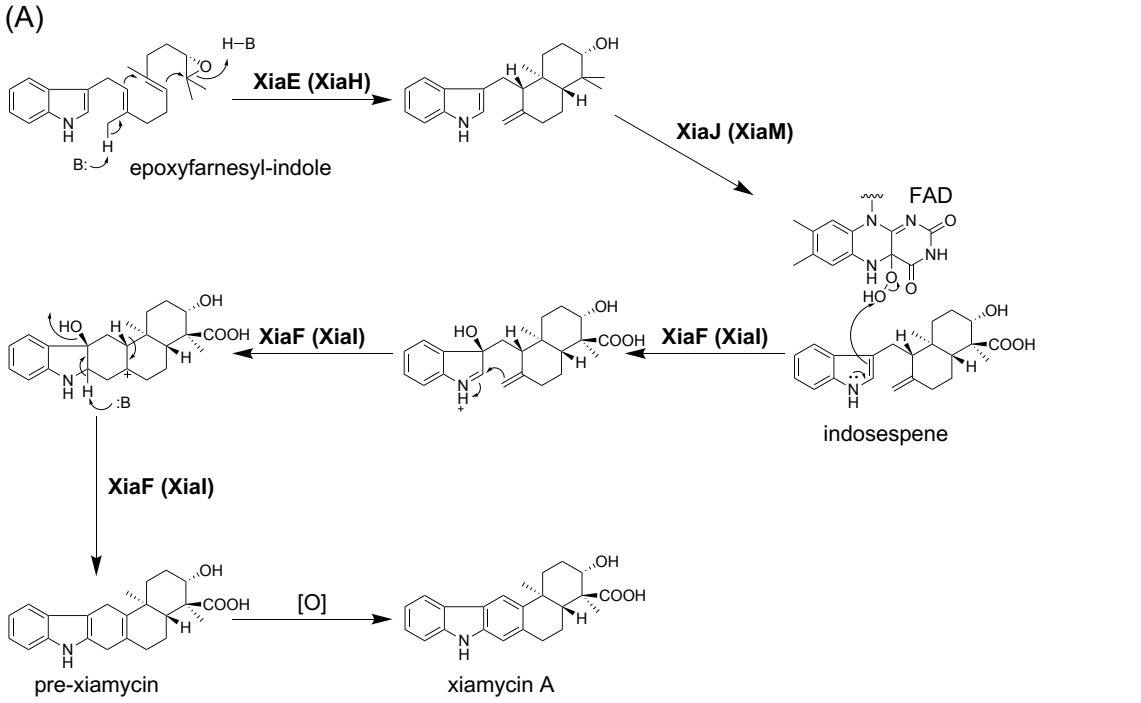
(A)
XiaE (XiaH)
epoxyfarnesyl-indole
XiaJ (XiaM)
FAD
indosespene
XiaF (XiaI)
XiaF (XiaI)
XiaF (XiaI)
pre-xiamycin
[O]
xiamycin A

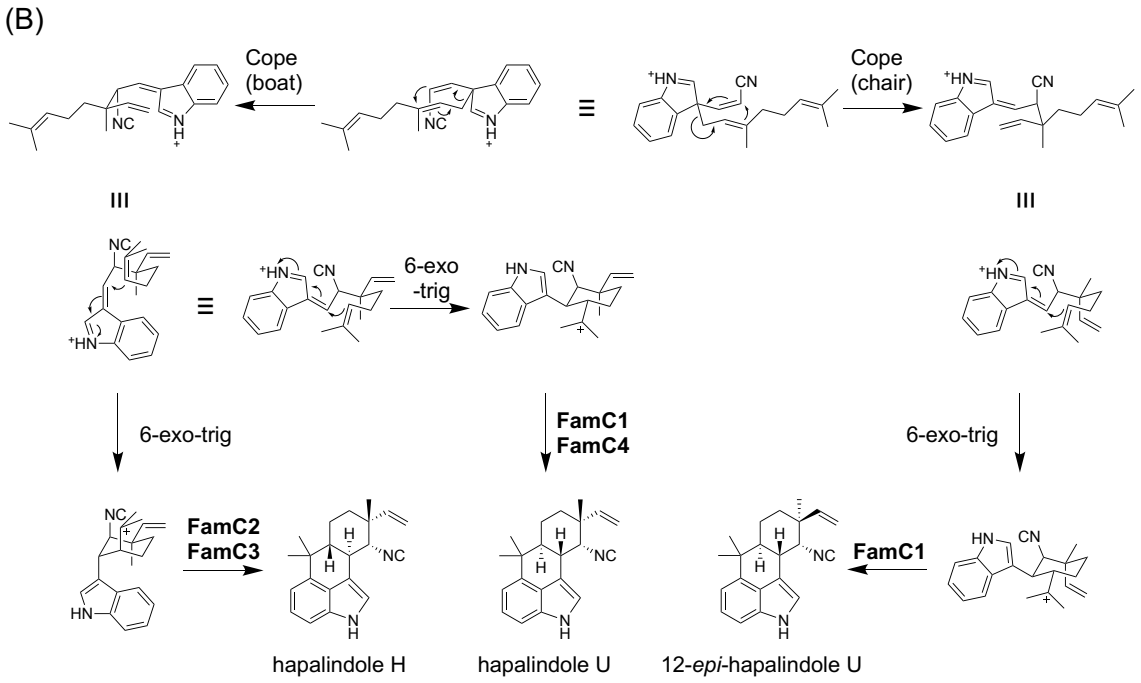
(B)
Cope (boat)
Cope (chair)
III
III
6-exo -trig
6-exo-trig
6-exo-trig
FamC1 FamC4
FamC2 FamC3
FamC1
hapalindole H
hapalindole U
12-epi-hapalindole U

(C)

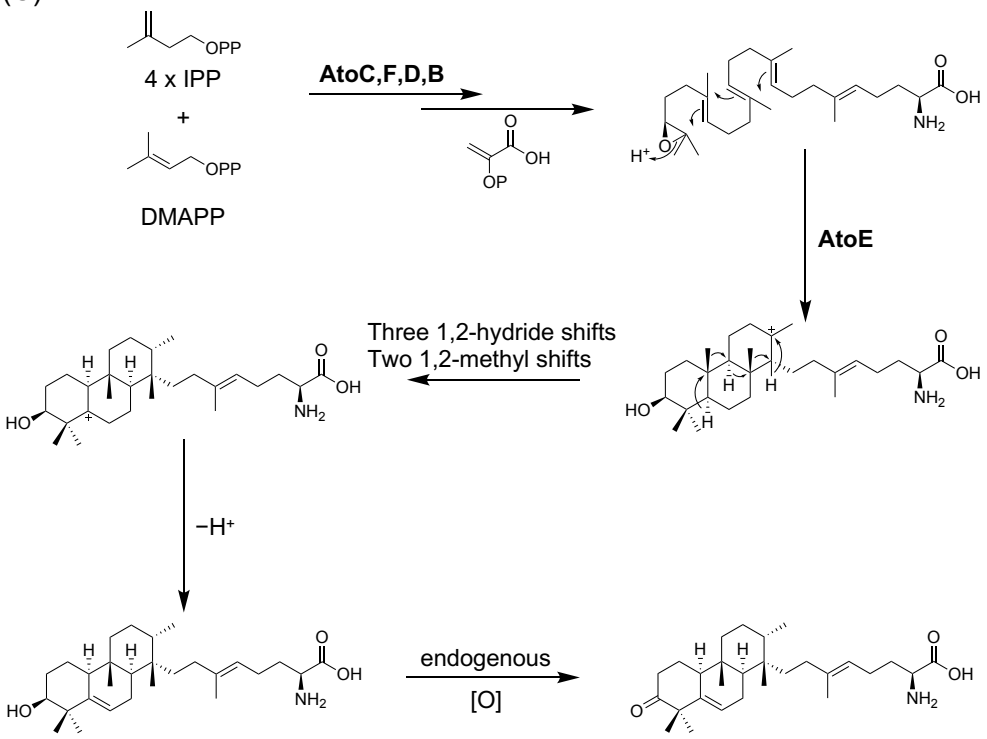

Figure S3. Unique cyclization mechanisms of bacterial meroterpenoids.

(A) The indolesesquiterpenoid xiamycins undergo two distinct cyclizations to form their pentacyclic core. First, the integral membrane protein XiaE/XiaH (independently named) rearranges 3-(epoxyfarnesyl)-indole to yield a decalin intermediate, and then the FAD-dependent oxidase XiaF/XiaI catalyzes a second ring closure that ultimately leads to pre-xiamycin and, after further oxidation, to xiamycin A. (B) The hapalindoles, a family of polycyclic indole-terpenoids from cyanobacteria, undergo Cope rearrangement–initiated cyclizations mediated by the Stig cyclases. FamC1 catalyzes a three-step cascade starting with a Cope rearrangement and followed by an aza-Prins cyclization to yield 12-epi-hapalindole U, while a 1:1 mixture of FamC2 and FamC3 predominantly produces hapalindole H (especially in the presence of Ca^{2+}), and a combination of FamC1 with FamC4 under pH 6.0 conditions shifts the reaction to favor the formation of hapalindole U. (C) The enzyme AtoE catalyzes the cyclization of meroterpenoids by protonating an epoxide group through its conserved xxxE314TAE motif, initiating a cascade of carbocation-driven reactions. Key aromatic and aliphatic residues in the active site stabilize the substrate and control the stereochemistry of the reaction. Mutational studies confirmed that E314 is crucial as Brønsted acid for this cyclization process.

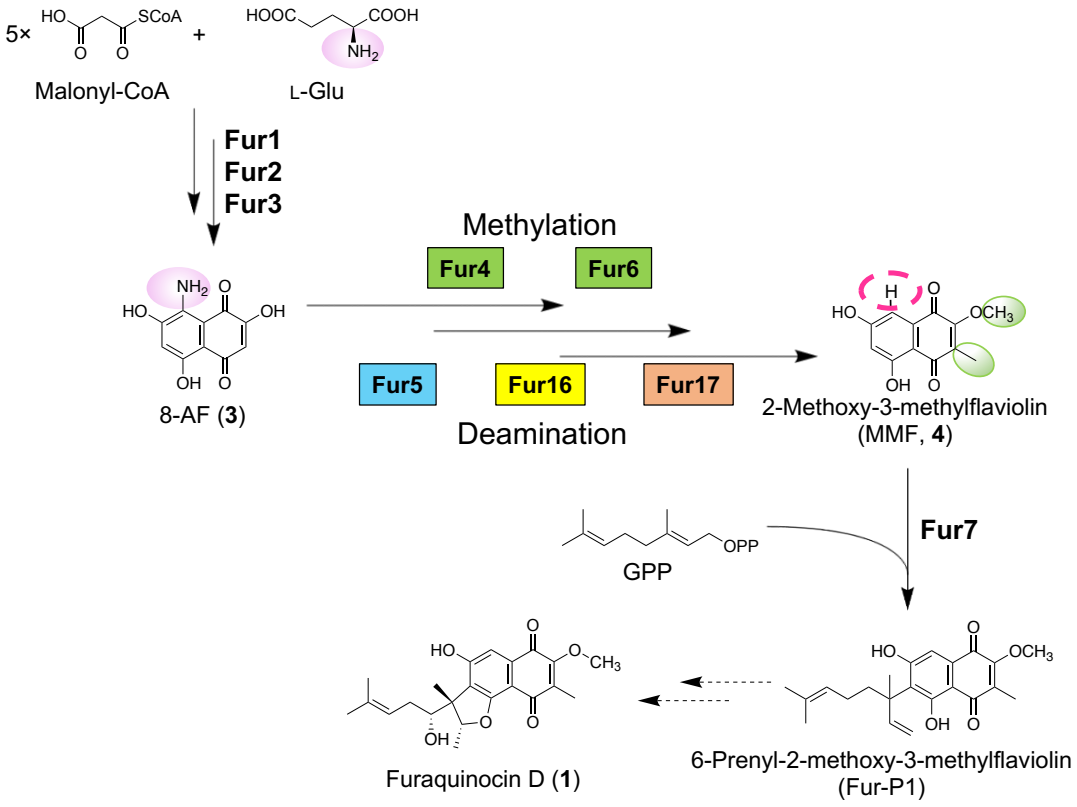

Figure S4. A previously proposed biosynthetic pathway for furaquinocin.

In addition to 8-AF (**3**), MMF (**4**) has been identified as a substrate for geranylation. During the conversion to **4** from **3**, two methylations and reductive deamination reactions occur.

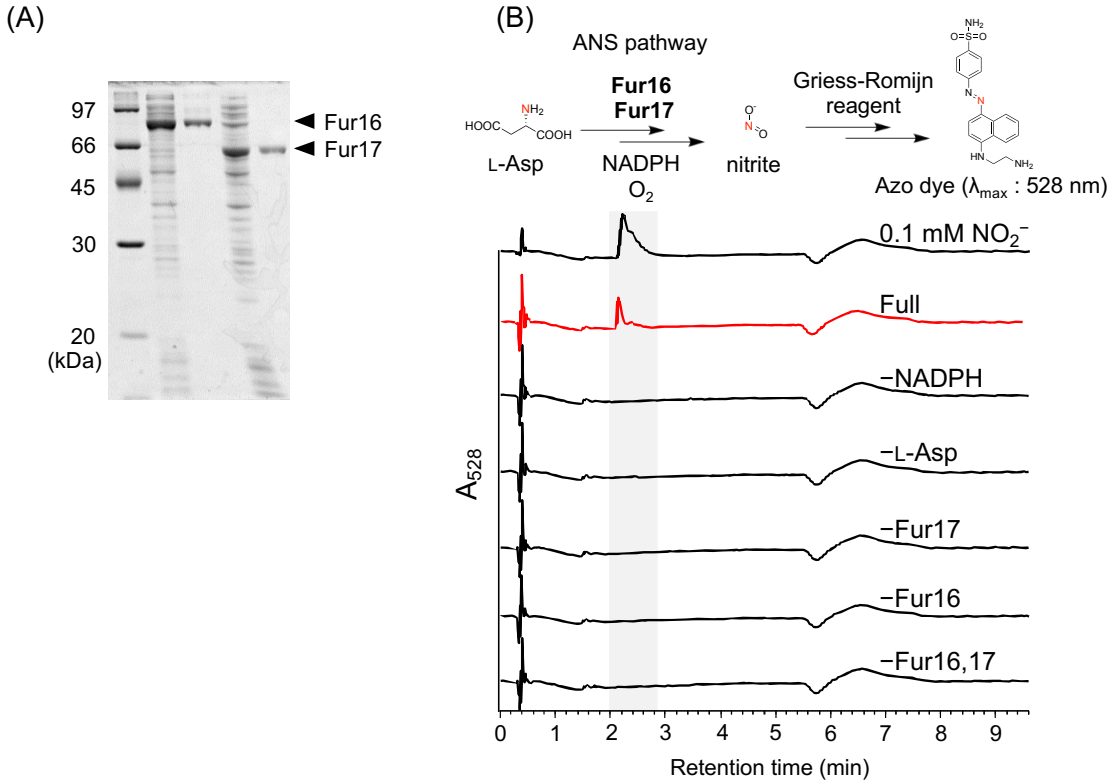

Figure S5. Nitrite production by Fur16 and Fur17.

(A) SDS–PAGE analysis of Fur16 and Fur17. The molecular weights of Fur16 and Fur17 are 71 kDa and 51 kDa, respectively. **(B)** HPLC–UV/VIS chromatograms of the Fur16 and Fur17 reaction mixture. A_{528}, absorbance at 528 nm. Nitrite was produced in a Fur16- and Fur17-dependent manner. The assay conditions are described in the Supporting Information.

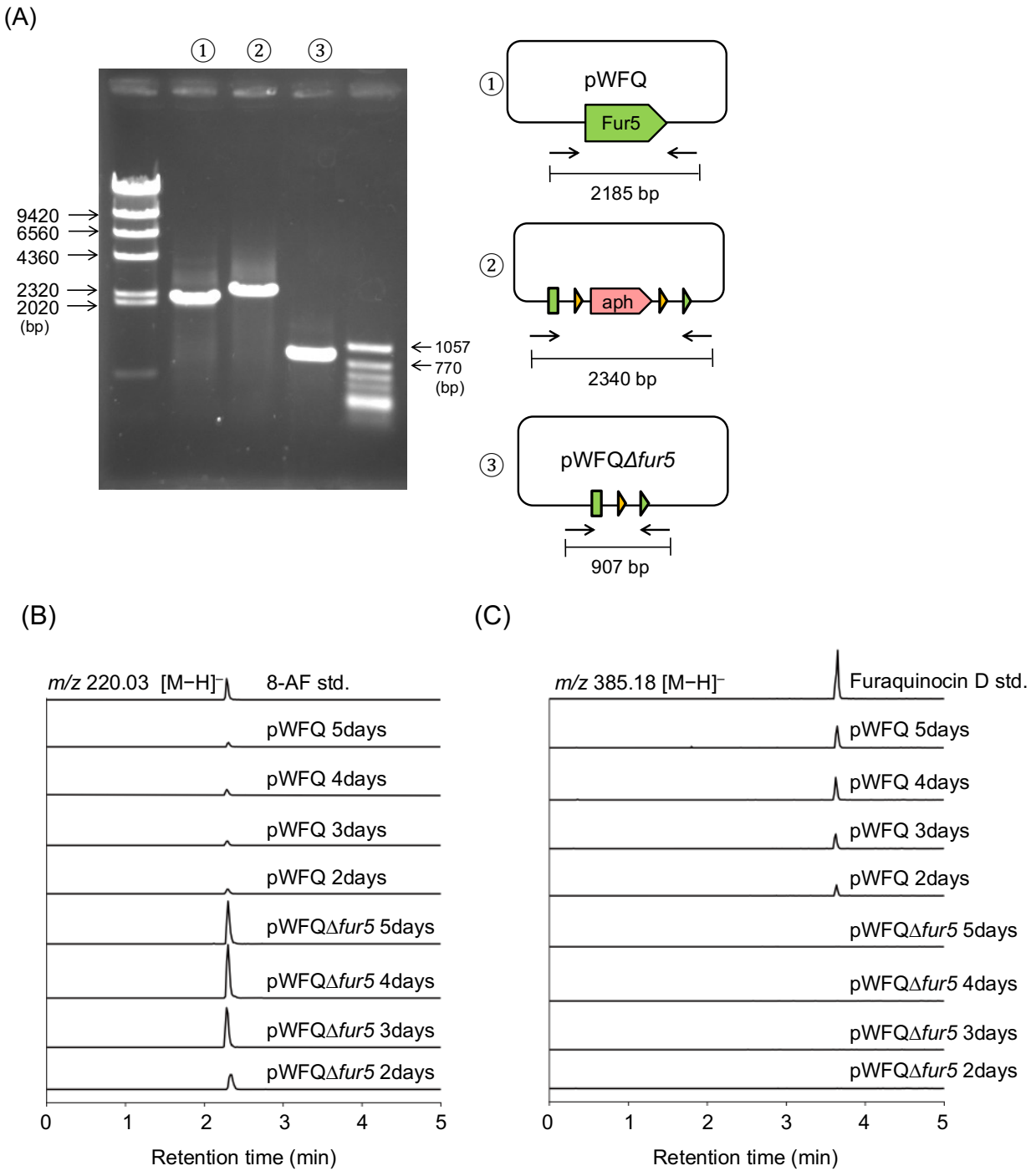

Figure S6. Gene disruption of *fur5* and heterologous expression analysis of pWFQΔ*fur5*.

(A) Gene disruption and confirmation of *fur5* gene on pWFQ vector. The *fur5* gene was disrupted in-frame, and disruption was confirmed by the amplified length of the region between the two primers d_fur5_check_f and d_fur5_check_r by PCR. (Table S2) (**B**)**(C)** Extracted ion chromatograms of culture broth of *S. albus* G153 transformed with pWFQ or pWFQΔ*fur5*. (**B:** 220.03 $[M-H]^-$ for 8-AF, **C**: 385.18 $[M-H]^-$ for Furaquinocin D).

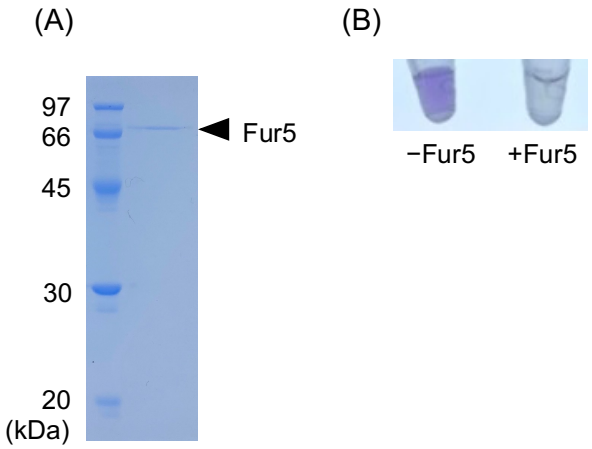

Figure S7. 8-AF consumption by Fur5.

(A) SDS–PAGE analysis of Fur5. The molecular weight of Fur5 is 59 kDa. **(B)** Fur5 reaction mixture after the 1 h of incubation. The 8-AF-derived purple color disappeared after incubation with Fur5. The assay conditions are described in the Supporting Information.

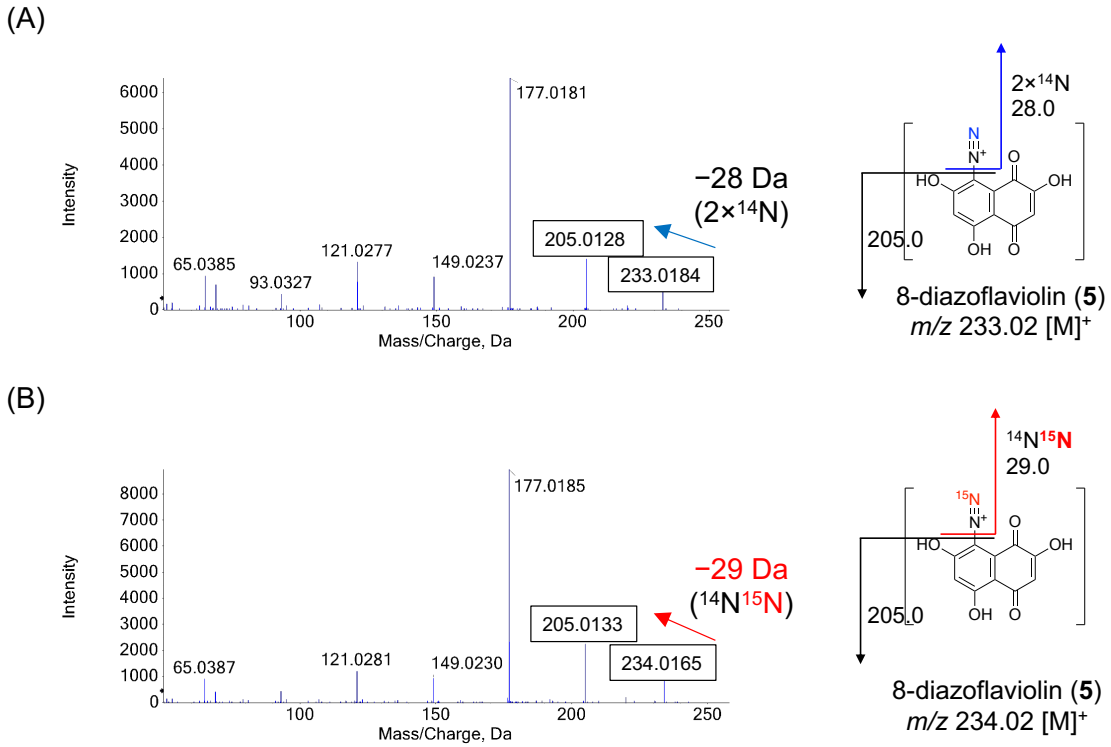

Figure S8. LC–MS/MS analysis of 8-diazoflaviolin.

(A) MS/MS spectrum of 8-diazoflaviolin (**5**) in the Fur5 reaction mixture. **(B)** MS/MS spectrum of ^{15}N labeled 8-diazoflaviolin (**5**) in the Fur5 reaction mixture with ^{15}N-labeled nitrite.

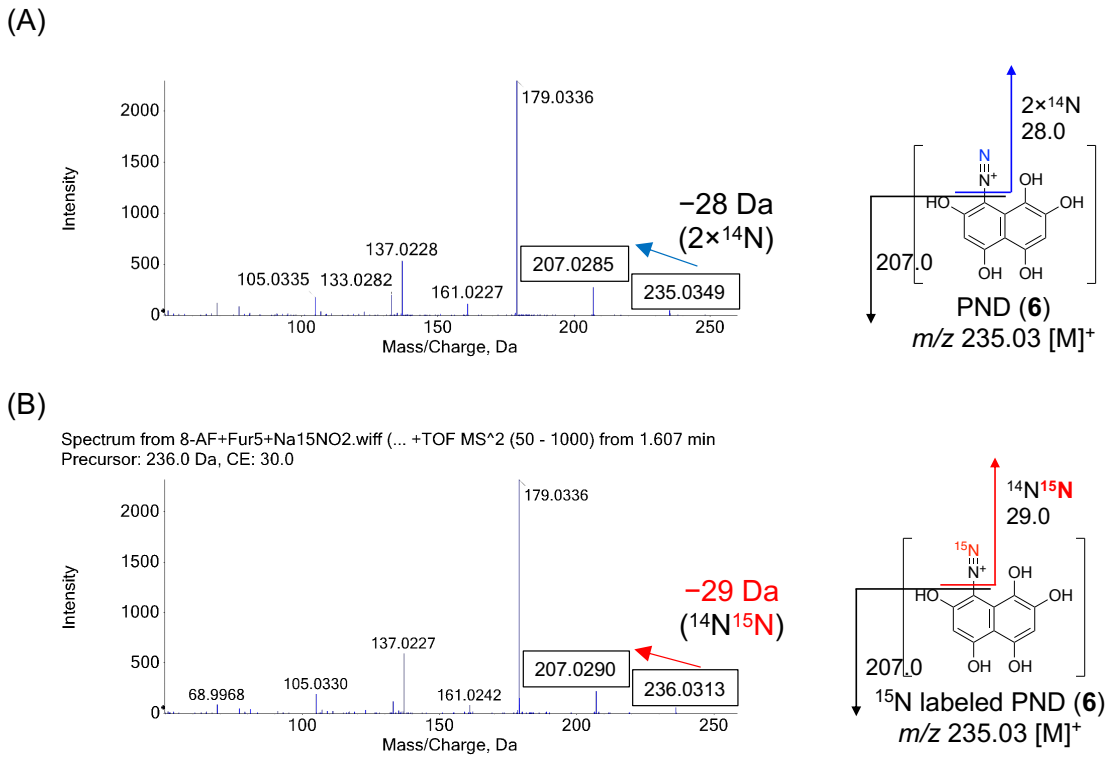

Figure S9. LC–MS/MS analysis of PND.

(A) MS/MS spectrum of PND (**6**) in the Fur5 reaction mixture. **(B)** MS/MS spectrum of ^{15}N-labeled PND (**6**) in the Fur5 reaction mixture with ^{15}N-labeled nitrite.

(A)

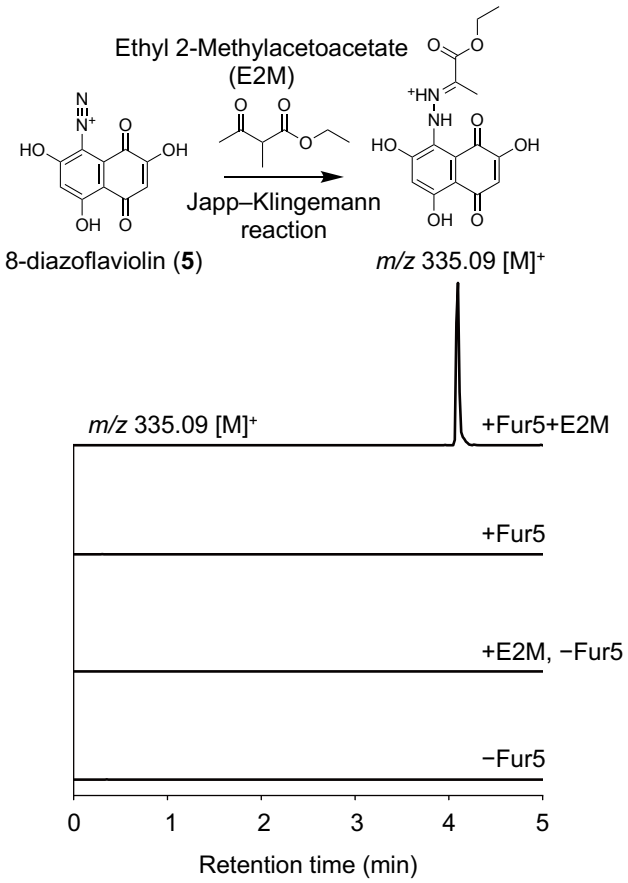

(B)

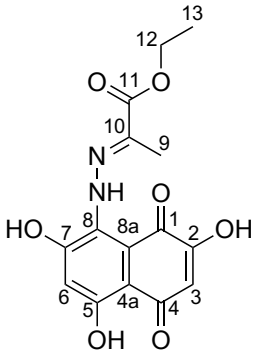

No.	δ_H (ppm) (multi, J_H (Hz))
3	5.60 (s)
6	6.55 (s)
9	2.22 (s)
12	4.28 (q, 7.3)
13	1.33 (t, 7.1)
	CD_3OD

^{1}H NMR (600 MHz)
(in CD_3OD)

(C)

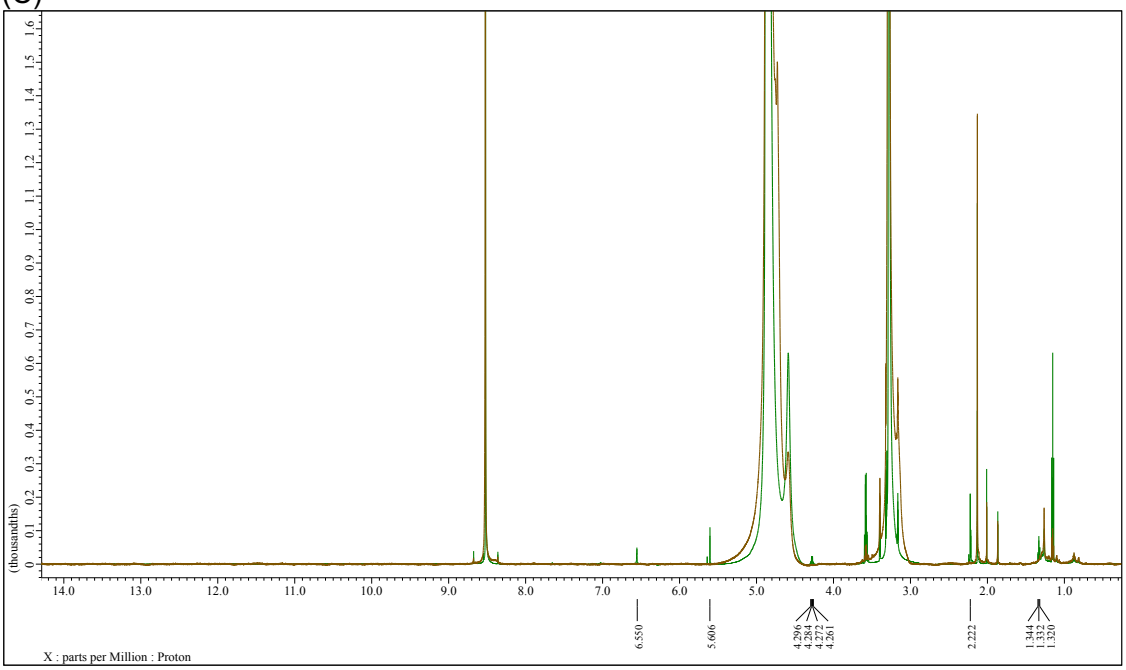

Figure S10. Structural analyasis of derivatized 8-diazoflaviolin.

(A) Extracted ion chromatograms of derivatized 8-diazoflaviolin in a Fur5 and ethyl 2-methylacetate dependent manner (335.09.03 $[M]^+$). **(B)(C)** ^{1}H NMR data of derivatized 8-diazoflaviolin. The green line is a ^{1}H NMR spectrum of derivatized 8-diazoflaviolin. The brown line is a ^{1}H NMR spectrum of blank fraction (Fractionation of the mobile phase only, as when derivatized **5** was fractionated) of preparative HPLC. The proton signals on the green line, which are not on the brown line, are listed in the table (B).

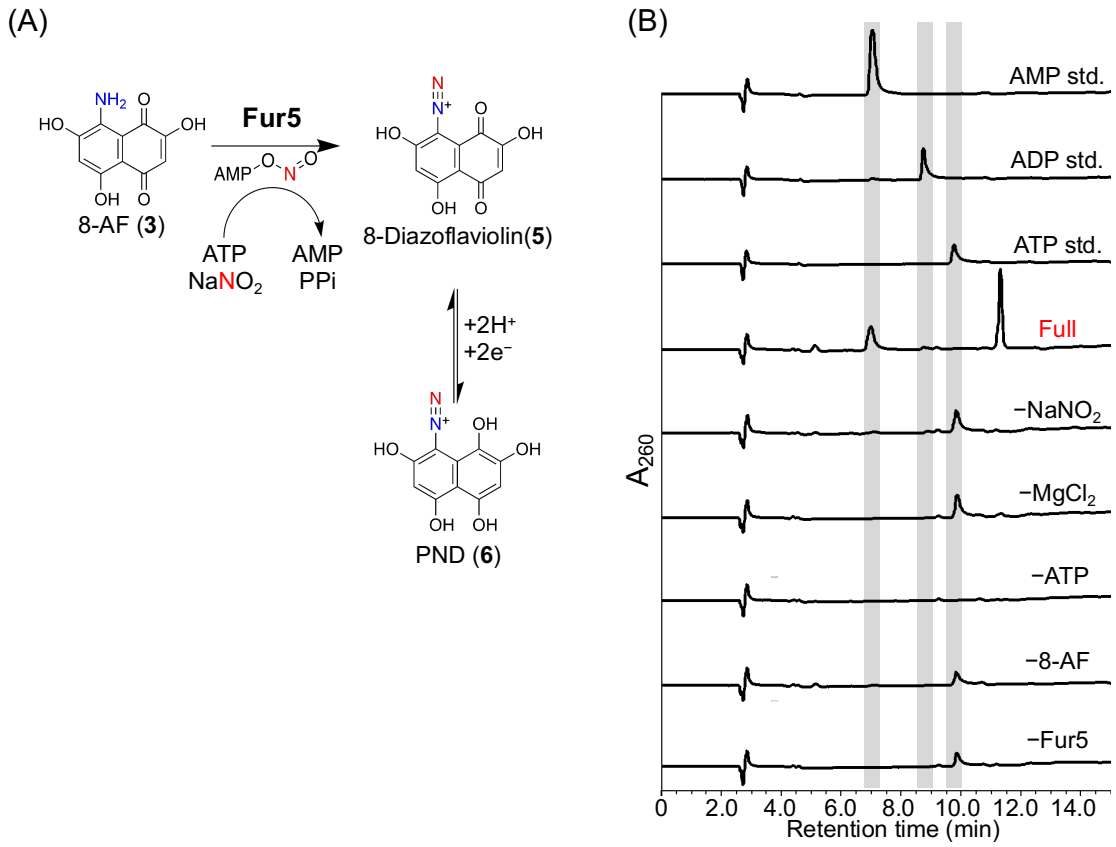

Figure S11. ATP consumption by Fur5.

(A) A proposed mechanism for the activation of ATP by Fur5. **(B)** HPLC–UV/VIS chromatograms of the Fur5 reaction mixture. A_{260}, absorbance at 260 nm. AMP was produced in an 8-AF-, ATP-, nitrite-, and Fur5-dependent manner. The assay conditions are described in the Supporting Information.

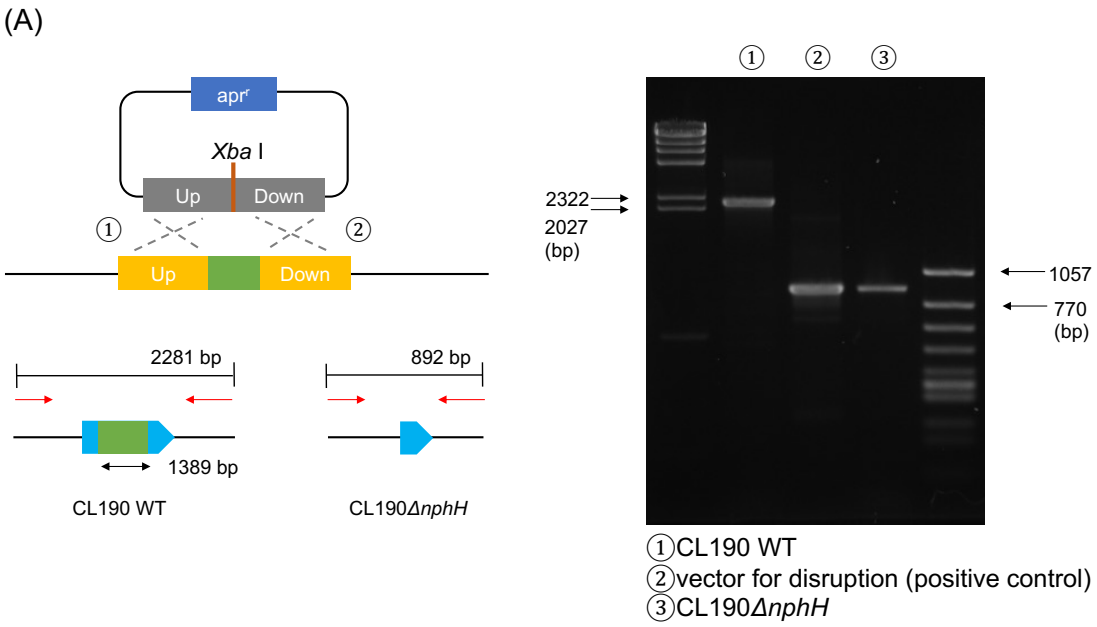
(A)
apr
Xba I
Up
Down
①
②
Up
Down
2281 bp
892 bp
1389 bp
CL190 WT
CL190ΔnphH
①
②
③
2322
2027
(bp)
1057
770
(bp)
①CL190 WT
②vector for disruption (positive control)
③CL190ΔnphH

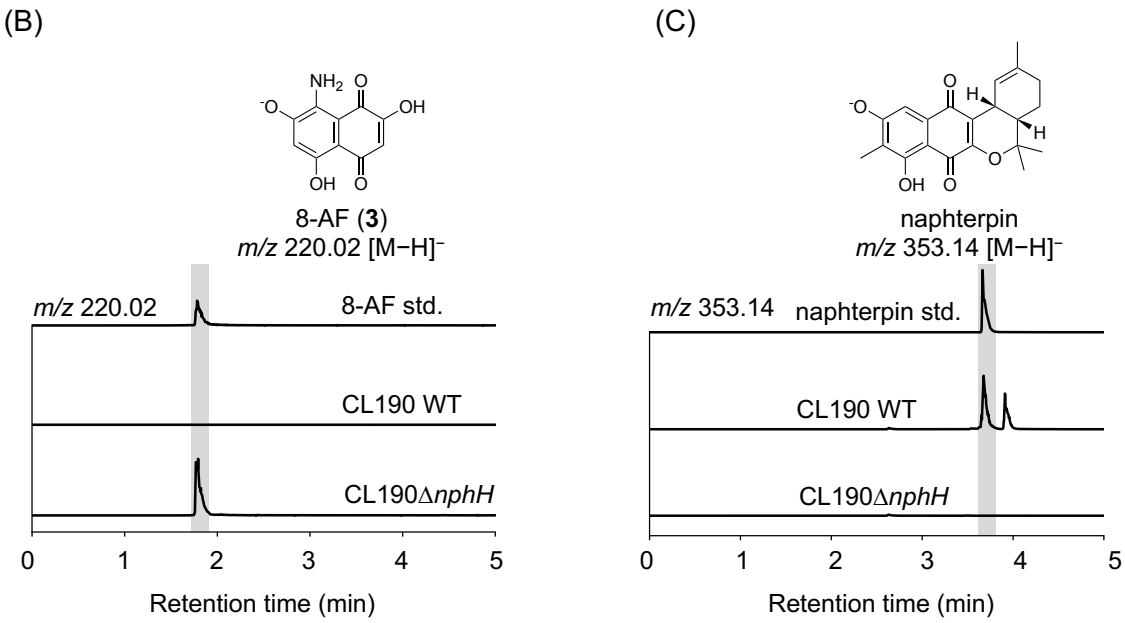
(B)
8-AF (3)
m/z 220.02 [M−H]⁻
m/z 220.02
8-AF std.
CL190 WT
CL190ΔnphH
0
1
2
3
4
5
Retention time (min)
(C)
naphterpin
m/z 353.14 [M−H]⁻
m/z 353.14
naphterpin std.
CL190 WT
CL190ΔnphH
0
1
2
3
4
5
Retention time (min)

(D)

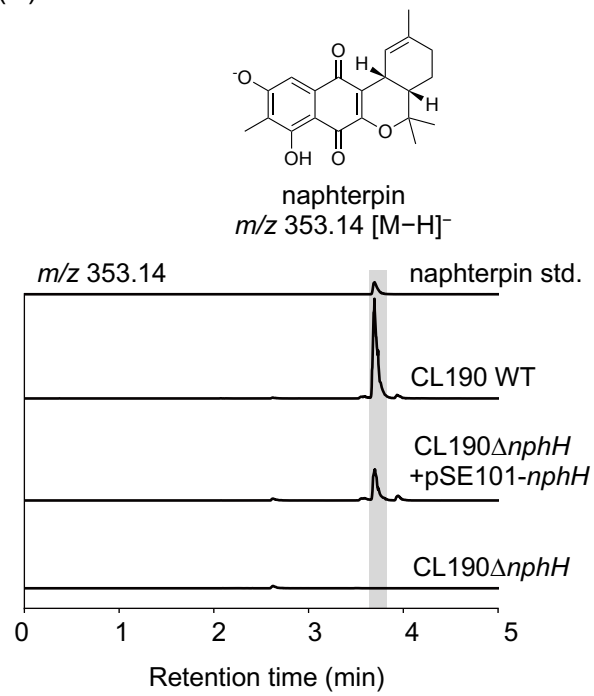

Figure S12. Gene disruption of *nphH* and heterologous expression analysis of *Streptomyces* sp. CL190Δ*nphH*.

(A) Gene disruption by double crossover and confirmation of *nphH* gene on the genome of CL190 strain. The *nphH* gene was disrupted in-frame, and disruption was confirmed by the amplified length of the region between the two primers d_nphH_check_f and d_nphH_check_r by PCR. (Table S2) **(B)(C)** Extracted ion chromatograms of culture broth (1day) of *S.* sp CL190wiletype (WT) and Δ*nphH* and Δ*nphH*+pSE101-*nphH* (complemented strain). (**B:** 220.03 $[M-H]^-$ for 8-AF, **C**: 353.14 $[M-H]^-$ for naphterpin). **(D)** Extracted ion chromatograms of culture broth (3days) of *S.* sp CL190wiletype (WT) and Δ*nphH* and Δ*nphH*+pSE101-*nphH* (complemented strain). (353.14 $[M-H]^-$ for naphterpin).

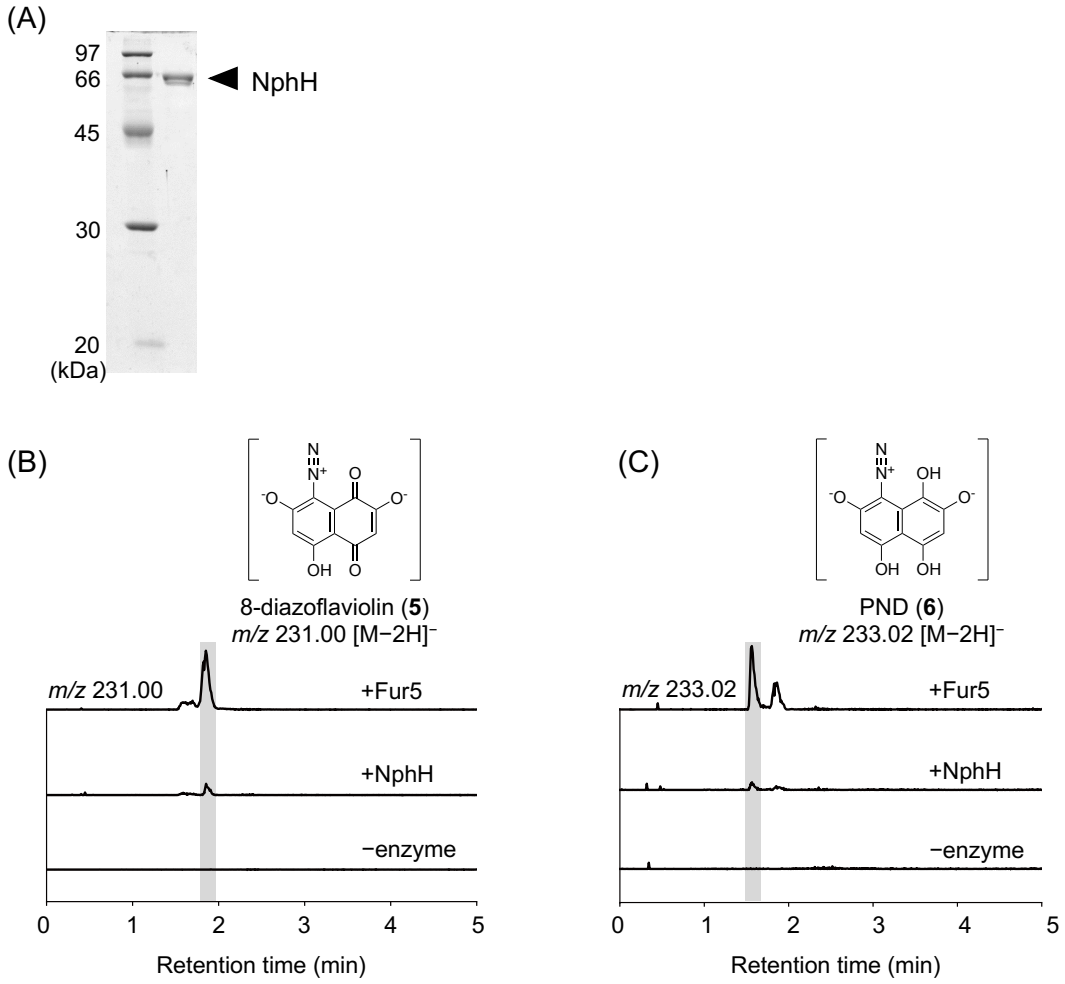

Figure S13. Diazotization of 8-AF by NphH, a homolog of Fur5

(A) SDS–PAGE analysis of NphH. The molecular weight of NphH is 59 kDa. **(B)(C)** LC–HRMS analysis of Fur5 or NphH reaction mixture. **5** and **6** were produced in a NphH-dependent manner as well as Fur5. The assay conditions are described in the Supporting Information. Compound **5** and **6** was detected by extracted ion chromatogram (XIC) (**B:** 231.00 $[M-2H]^-$ for **5**, **C**: 233.02 $[M-2H]^-$ for **6**).

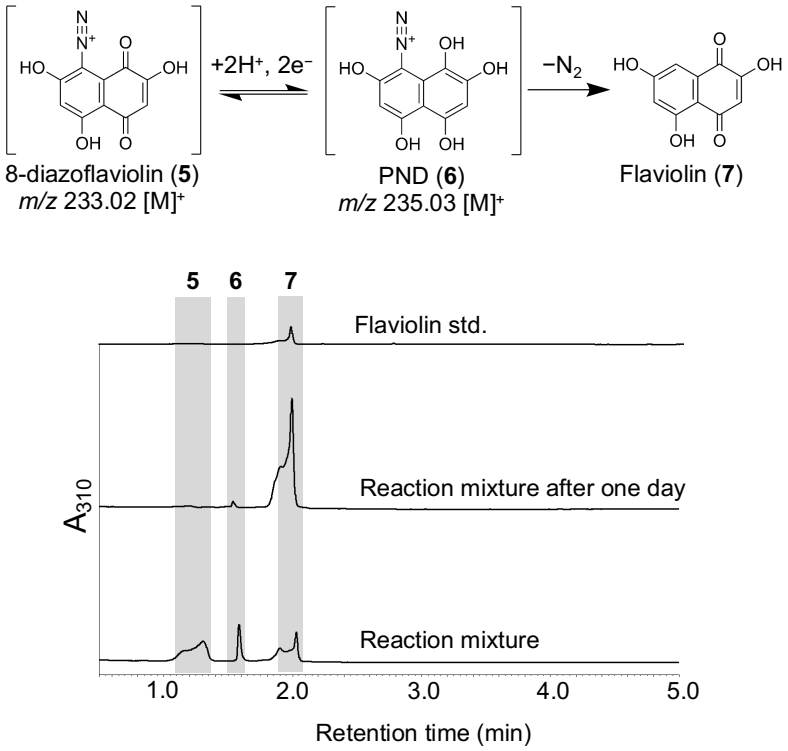

Figure S14. Time-dependent degradation of the diazo compounds.

A_{310}, absorbance at 310 nm. Both 8-diazoflaviolin (**5**) and PND (**6**) were degraded in a time-dependent manner and converted into flaviolin (**7**).

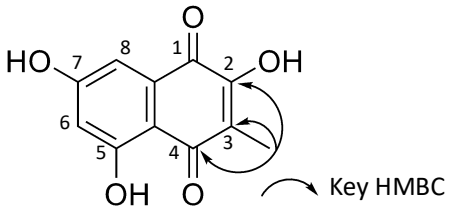

3-Methylflaviolin
(3-MF, **8**)

No.	δ_H (ppm) (multi, J_H (Hz))	δC (ppm)
1		180.1
2		156.0
3		119.1
3-Me	1.87 (s)	7.94
4		189.6
4a		131.9
5-OH	12.6 (s)	
5		162.8
6	6.50 (d, 3.0)	108.0
7		163.4
8	6.93 (d, 3.0)	107.8
8a		107.3
OH	10.9 (s)	
		$(CD_3)_2SO$-d_6

^{1}H NMR (600 MHz)
^{13}C NMR (150 MHz)
(in $(CD_3)_2SO$)

^{1}H NMR

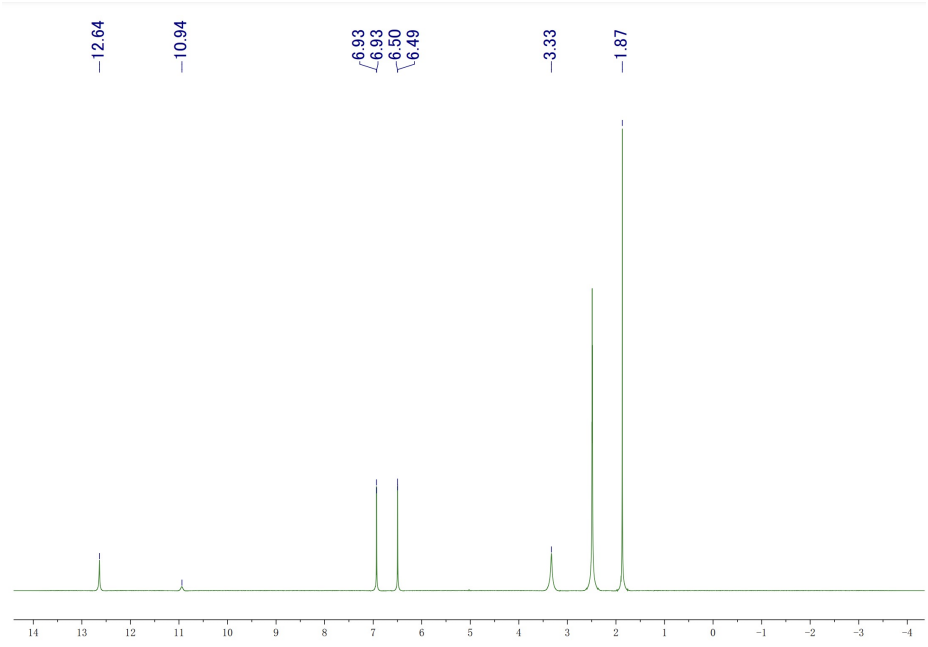
12.64
10.94
6.93
6.93
6.50
6.49
3.33
1.87
14
13
12
11
10
9
8
7
6
5
4
3
2
1
0
−1
−2
−3
−4

^{13}C NMR

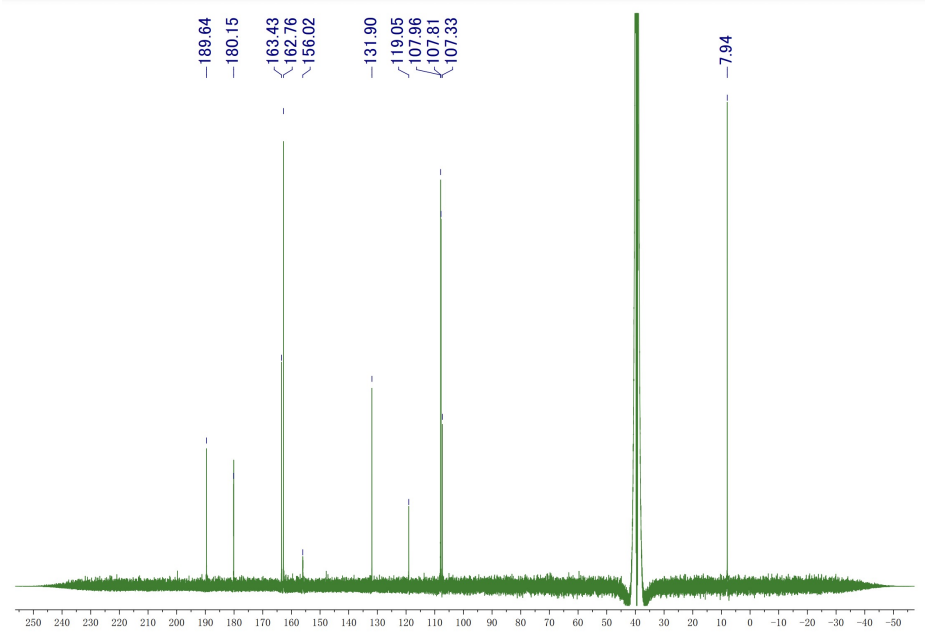
189.64
180.15
163.43
162.76
156.02
131.90
119.05
107.96
107.81
107.33
7.94
250 240 230 220 210 200 190 180 170 160 150 140 130 120 110 100 90 80 70 60 50 40 30 20 10 0 -10 -20 -30 -40 -50

HSQC

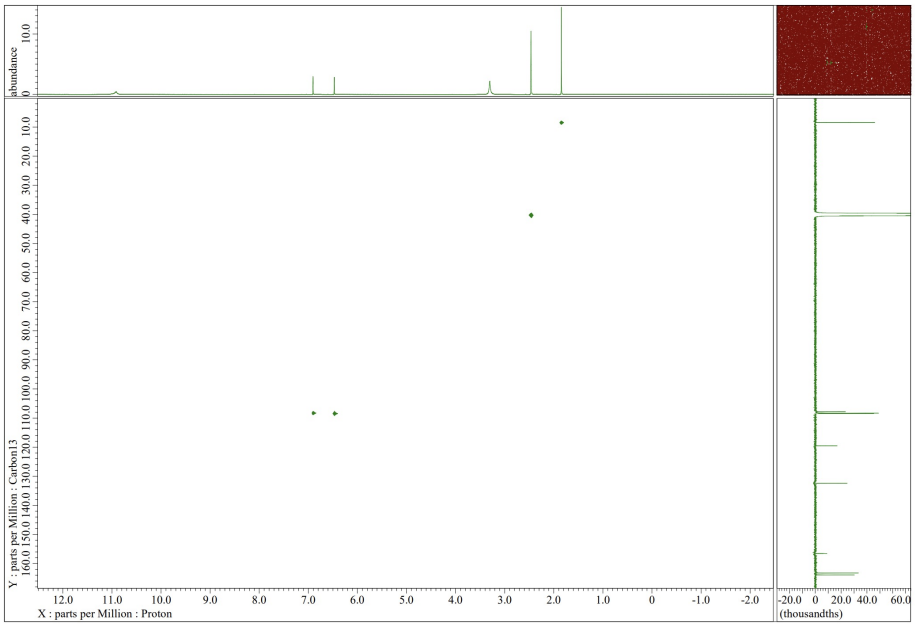
abundance
0
10.0
Y : parts per Million : Carbon13
10.0
20.0
30.0
40.0
50.0
60.0
70.0
80.0
90.0
100.0
110.0
120.0
130.0
140.0
150.0
160.0
12.0
11.0
10.0
9.0
8.0
7.0
6.0
5.0
4.0
3.0
2.0
1.0
0
-1.0
-2.0
X : parts per Million : Proton
-20.0
0
20.0
40.0
60.0
(thousandths)

HMBC

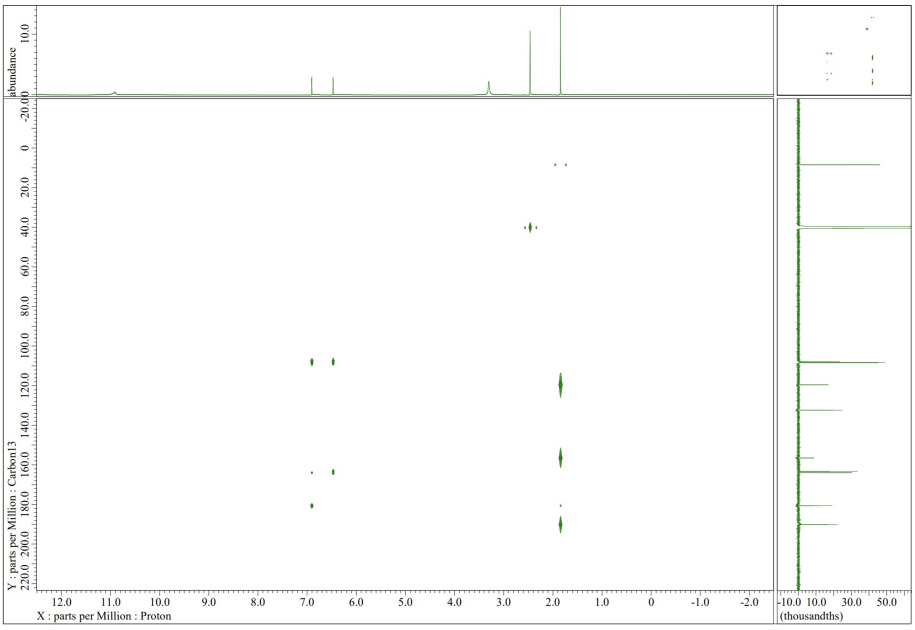

Figure S15. NMR spectra of 3-MF.

1D spectra of ^{1}H and ^{13}C, 2D spectra of HSQC and HMBC, and the summarized table of the NMR spectra of 3-MF (**8**).

(A) (B)

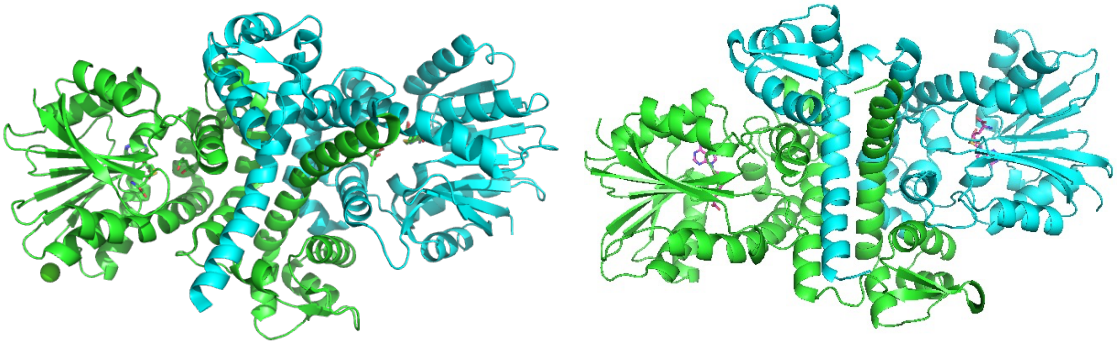

Mitomycin 7-*O*-methyltransferase MmcR Fur6

Figure S16. Structure comparison between Fur6 and a known methyltransferase.

(A) Structure of mitomycin 7-*O*-methyltransferase MmcR (59 % identity with Fur6). **(B)** Structure of Fur6. The crystal structure of Fur6 is similar to that of MmcR (RMSD 4.4 Å). SAH is accommodated in the active site. The N-terminal domain has a dimerization function.

PHN structure	Position	pK_a
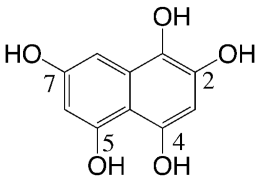	2-OH	8.02
	4-OH	6.80
	5-OH	6.74
	7-OH	9.27

Figure S17. Predicted p*Ka* of the hydroxy group in PHN.

The p*Ka* values of the hydroxy groups at each position are shown in the right column.

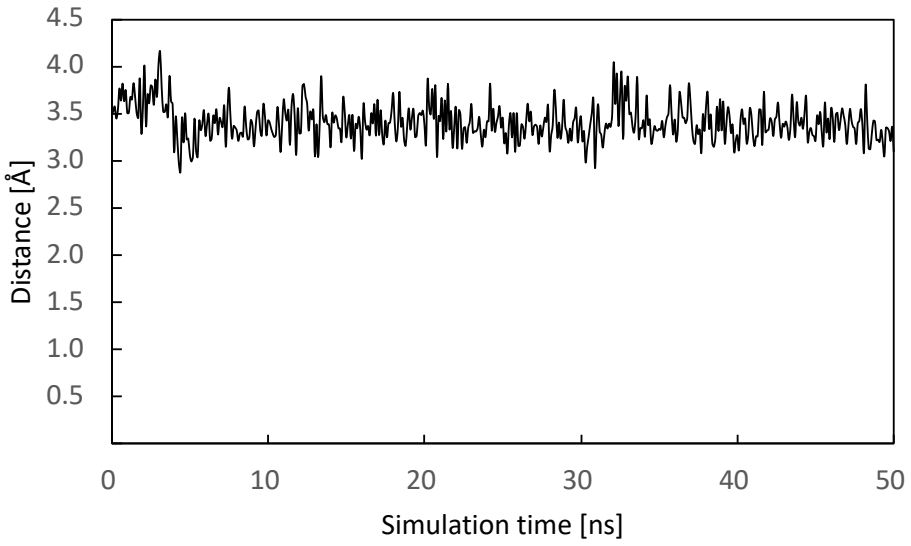

Figure S18. Plot of the distance between the methyl group of SAM and C3 of PHN. The plot was obtained from the unstrained 50-ns MD simulation.

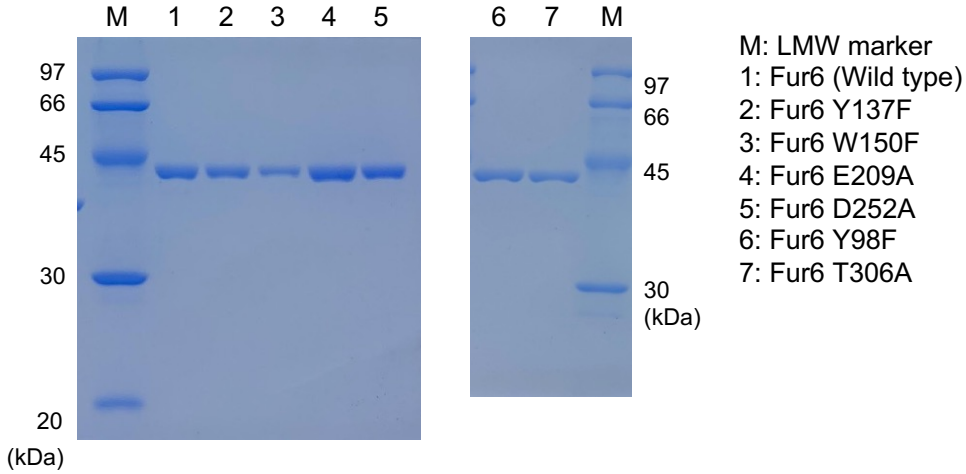

Figure S19. Fur6 and its variants expression.

SDS–PAGE analysis of Fur6 and its variants. All variants were prepared with homogeneity.

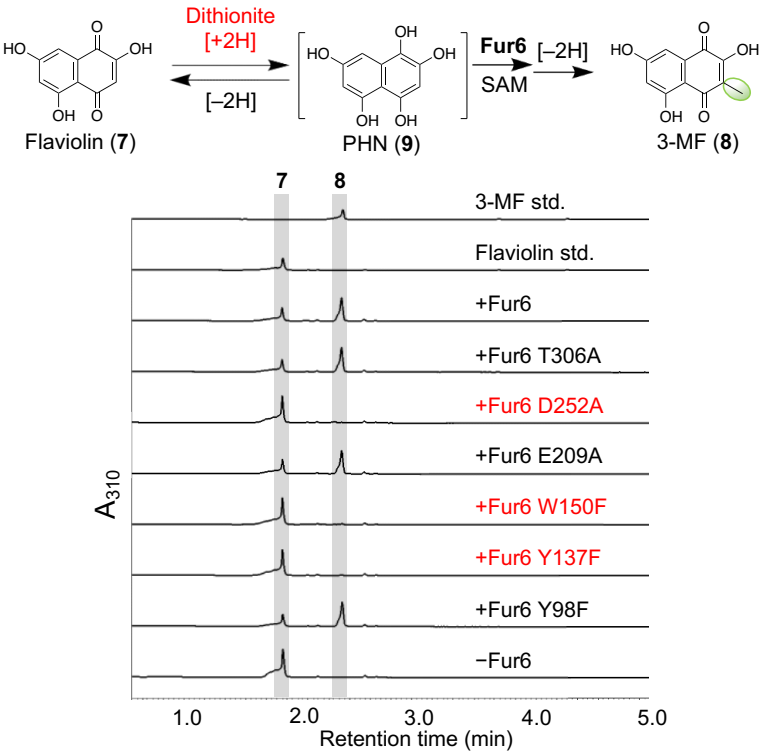

Figure S20. Methylation analysis of Fur6 variants.

The LC–UV/VIS chromatograms of the wild-type Fur6 and its variants reaction mixtures. A_{310}, absorbance at 310 nm. Methylation by Fur6 proceeded under reduced conditions, in which flaviolin (**7**) is reduced to PHN (**9**). The mutations, Y137F, W150F, and D252A, impaired Fur6 function, suggesting that these residues are essential for PHN recognition.

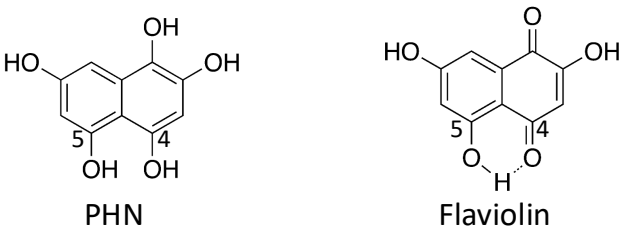

Figure S21. Structural comparison of PHN and flaviolin.

In the flaviolin structure, the hydroxy group at C5 forms a hydrogen bond with the ketone at C4, making it difficult to deprotonate.

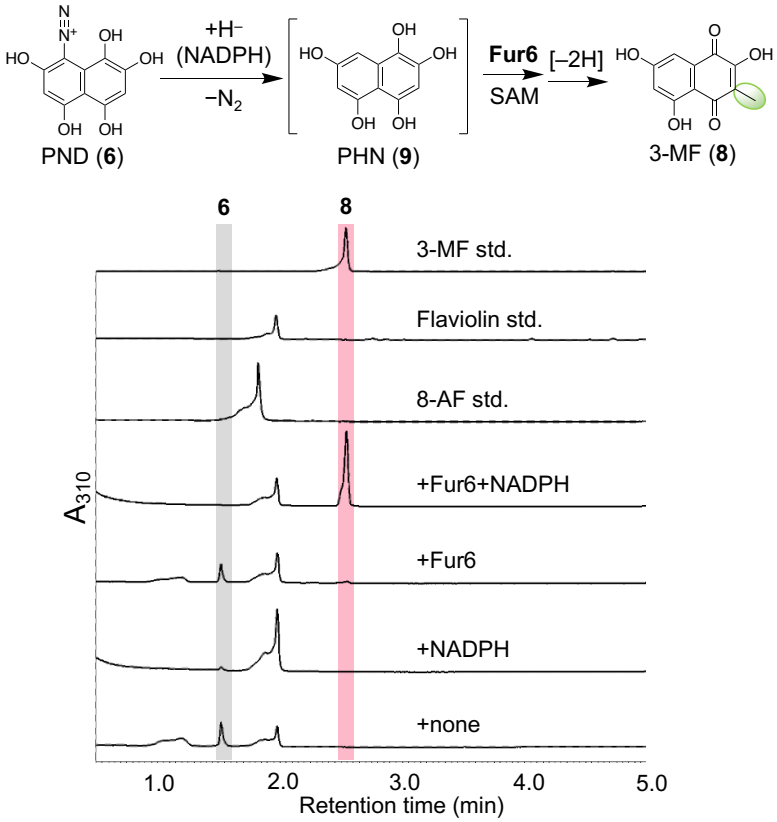

Figure S22. In vitro assays for the sequential Fur5 and Fur6 reaction mixture.

HPLC–UV/VIS analysis of the sequential Fur5 and Fur6 reaction mixture. A_{310}, absorbance at 310 nm. PHN (**9**) is generated by nonenzymatic reduction of **6** by the action of NADPH and served as a substrate for Fur6, resulting in methylation at C3 and the subsequent formation of **8** by air oxidation. The assay conditions are described in the Supporting Information.

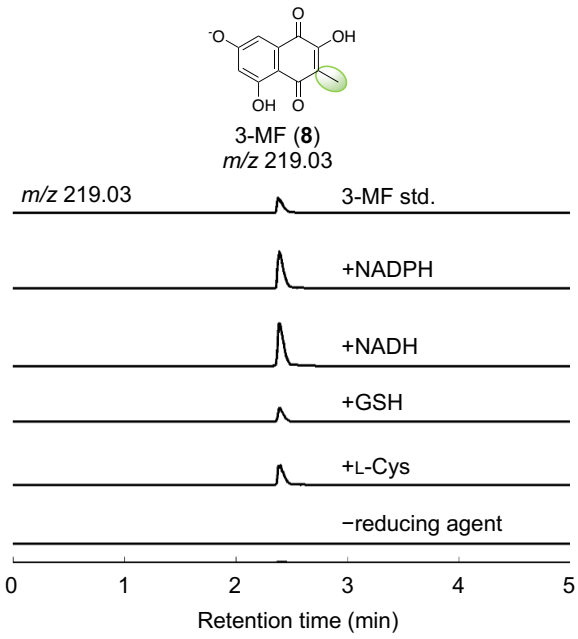

Figure S23. In vitro assays for the sequential Fur5 and Fur6 reaction mixture with a wide range of reducing agents.

LC–HRMS analysis of the sequential Fur5 and Fur6 reaction mixture. The assay conditions are described in the Supporting Information. Compound **8** was detected by extracted ion chromatogram (XIC) at *m/z* 219.03. GSH, glutathione.

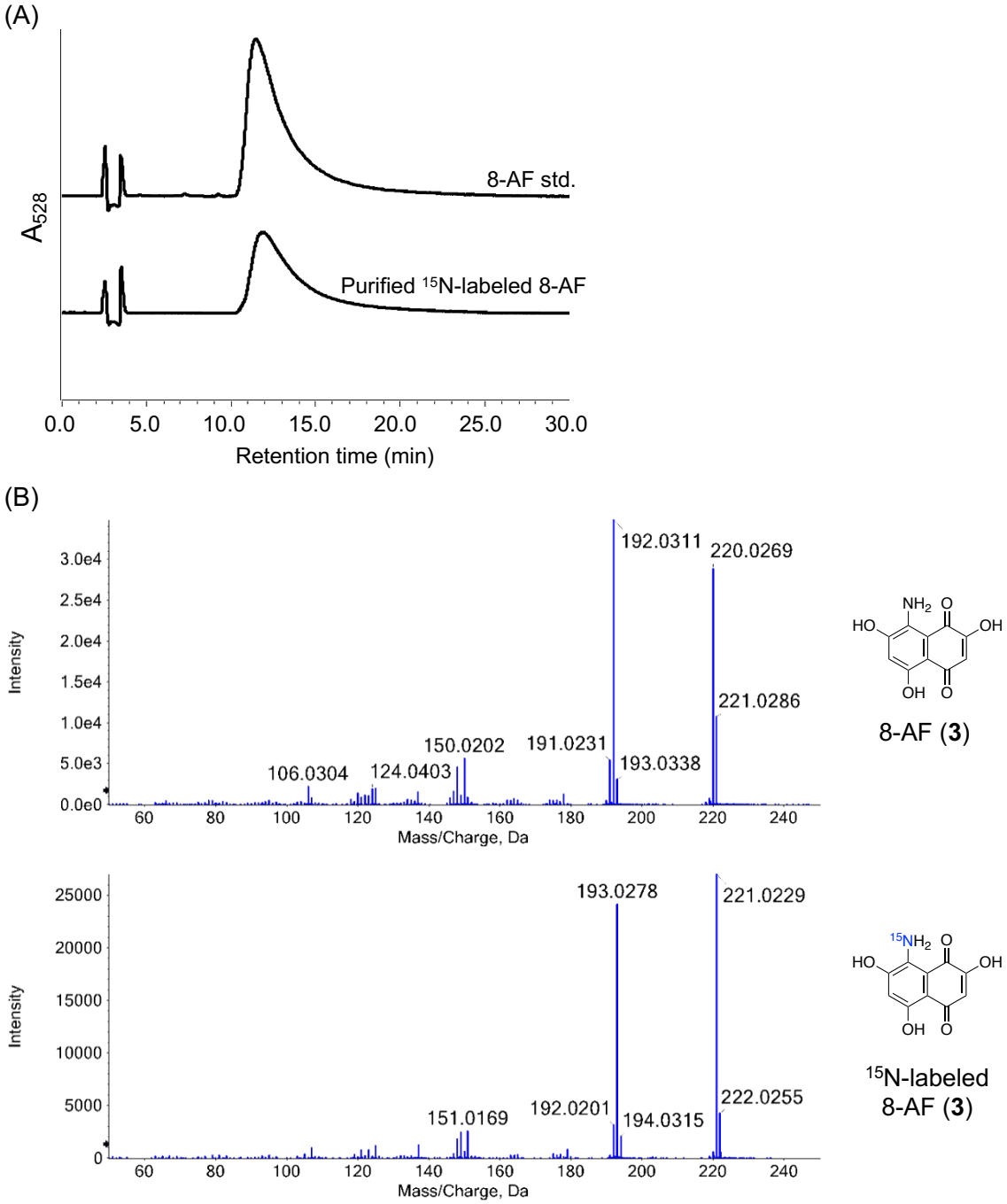

Figure S24. Spectra of ^{15}N-labeled 8-AF.

(A) HPLC–UV/VIS chromatograms of the 8-AF standard (upper) and purified the ^{15}N-labeled 8-AF (lower). A_{528}, absorbance at 528 nm. **(B)** MS/MS spectra of the 8-AF standard (upper) and purified ^{15}N-labeled 8-AF (lower). The purification conditions are described in the Supporting Information.

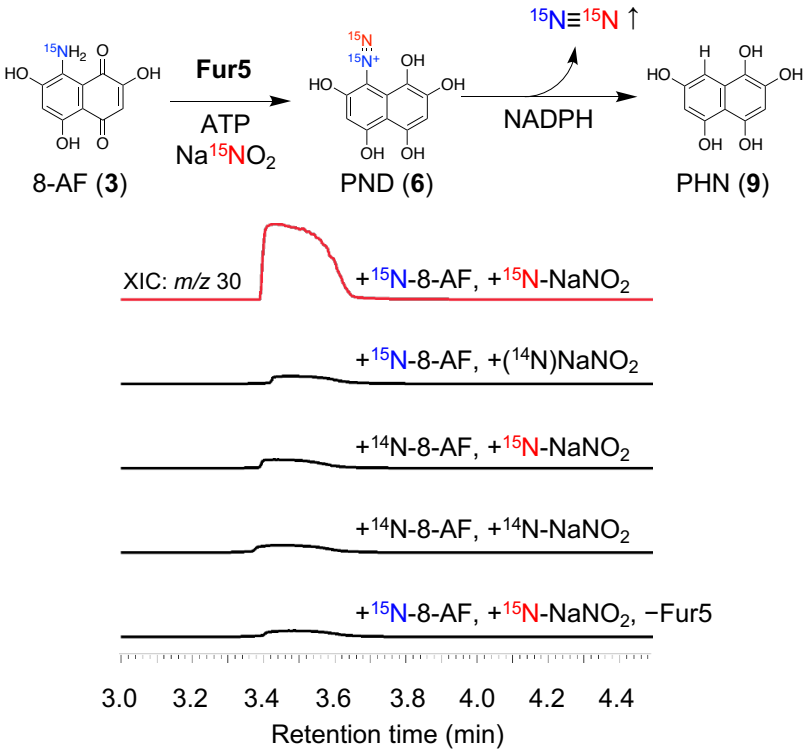

Figure S25. N_2 gas detection assays for the Fur5 and Fur6 reaction mixture.

GC–MS analysis of the Fur5 and Fur6 reaction mixture. Each peak was detected by extracted ion chromatogram at *m/z* 30. The assay conditions are described in the Supporting Information. Fully labeled N_2 gas ($^{15}N^{15}N$) was clearly detected under the "+^{15}N-8-AF, +^{15}N-$NaNO_2$" condition. In contrast, under the other conditions, negligible amounts of fully labeled N_2 gas ($^{15}N^{15}N$) were detected due to ^{15}N present in the natural 8-AF (3) or $NaNO_2$ at approximately 0.4 %.

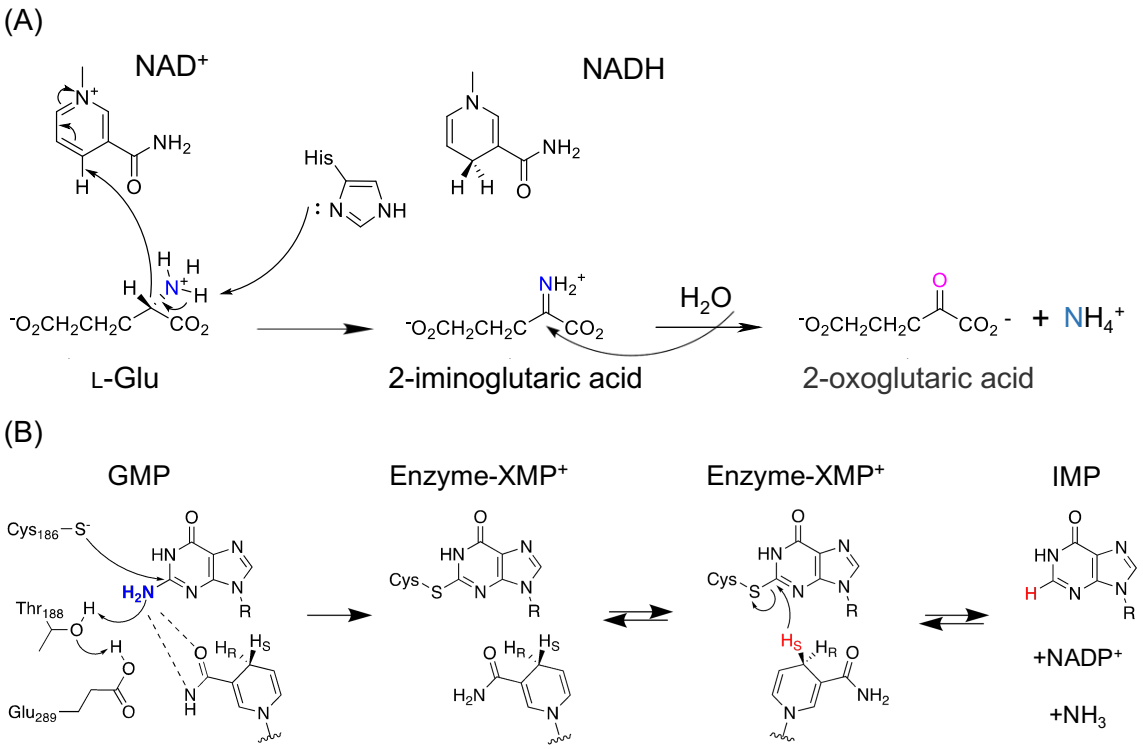

Figure S26. Comparison of deamination mechanisms *in vivo*.

(A) General deamination mechanisms by glutamate dehydrogenase *in vivo*. The amino group of L-Glu is oxidatively converted to the keto group of 2-oxoglutaric acid. **(B)** Proposed mechanism underlying the reductive deamination by the GMP reductase. In the reaction of GMP reductase, Cys186 binds to GMP, increasing the electrophilicity of the carbon atom and facilitating hydride reduction. GMP, 3-aminoavenalumic acid; XMP, xanthosine 5'-monophosphate; IMP, inosine 5'-monophosphate; AHA, 5-hydroxyanthranilate; DON, 6-diazo-5-oxo-L-norleucine.

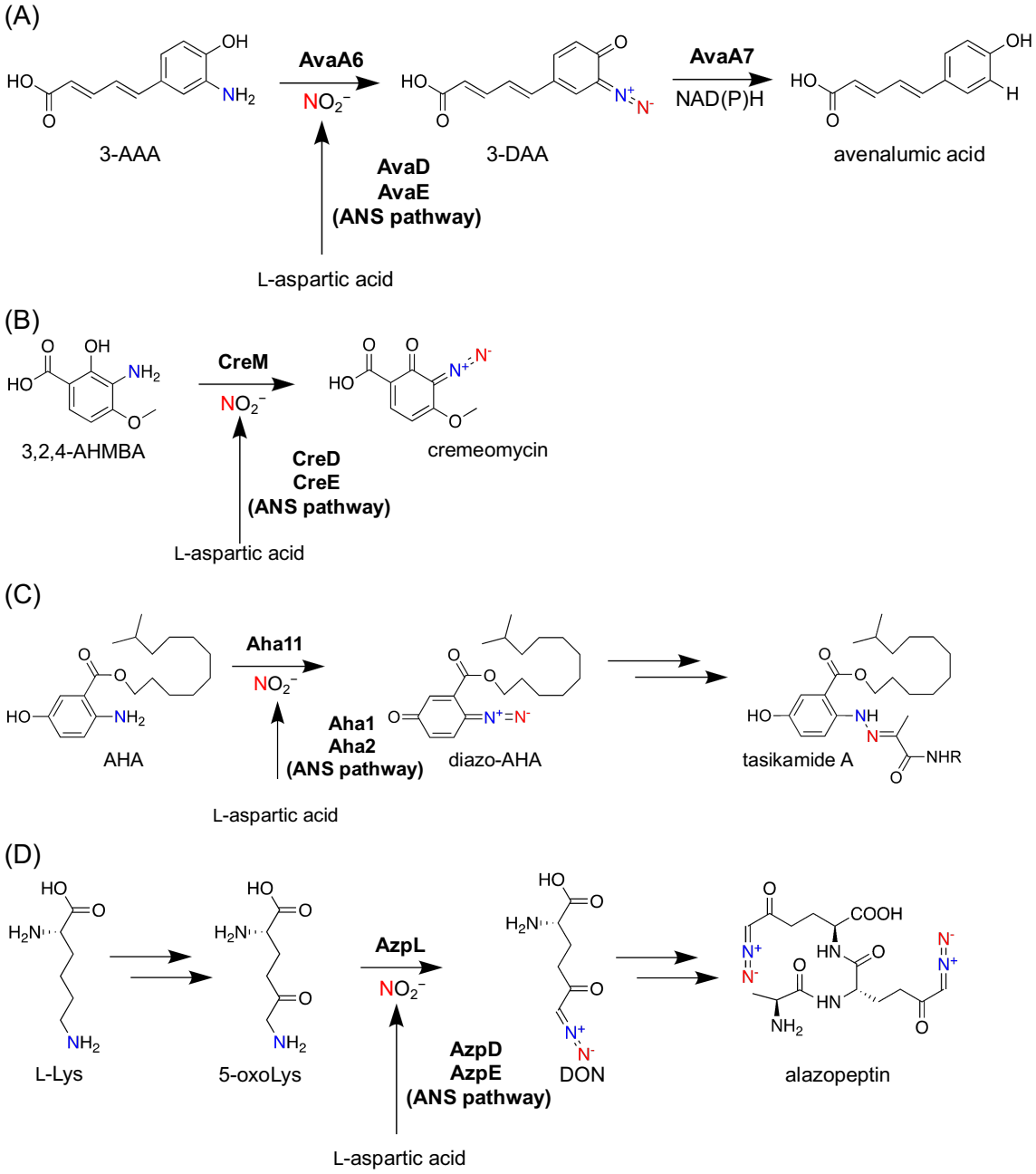

Figure S27. Diazo-forming enzymes and ANS pathway.

Representative ANS (L-aspartate-nitro-succinate) pathway that generates nitrous acid or nitrite from aspartate and characterized diazo-forming enzymes. **(A)** AvaA6 is the diazo-forming enzyme in the biosynthesis of avenalumic acid. Following diazotization by AvaA6, NAD(P)-dependent oxidoreductase AvaA7 achieves reductive deamination. **(B)** CreM is the diazo-forming enzyme in the biosynthesis of cremeomycin. **(C)** Aha11 is the diazo-forming enzyme in the biosynthesis of tasikamide. **(D)** AzpL is the diazo-forming enzyme in the biosynthesis of alazopeptin. All enzymes except AzpL are ATP-dependent enzymes. 3-AAA, 3-aminoavenalumic acid; 3-DAA, 3-diazoavenalumic acid; 3,2,4-AHMBA, 3-amino-2-hydroxy-4-methoxybenzoic acid; AHA, 5-hydroxyanthranilate; DON, 6-diazo-5-oxo-L-norleucine.

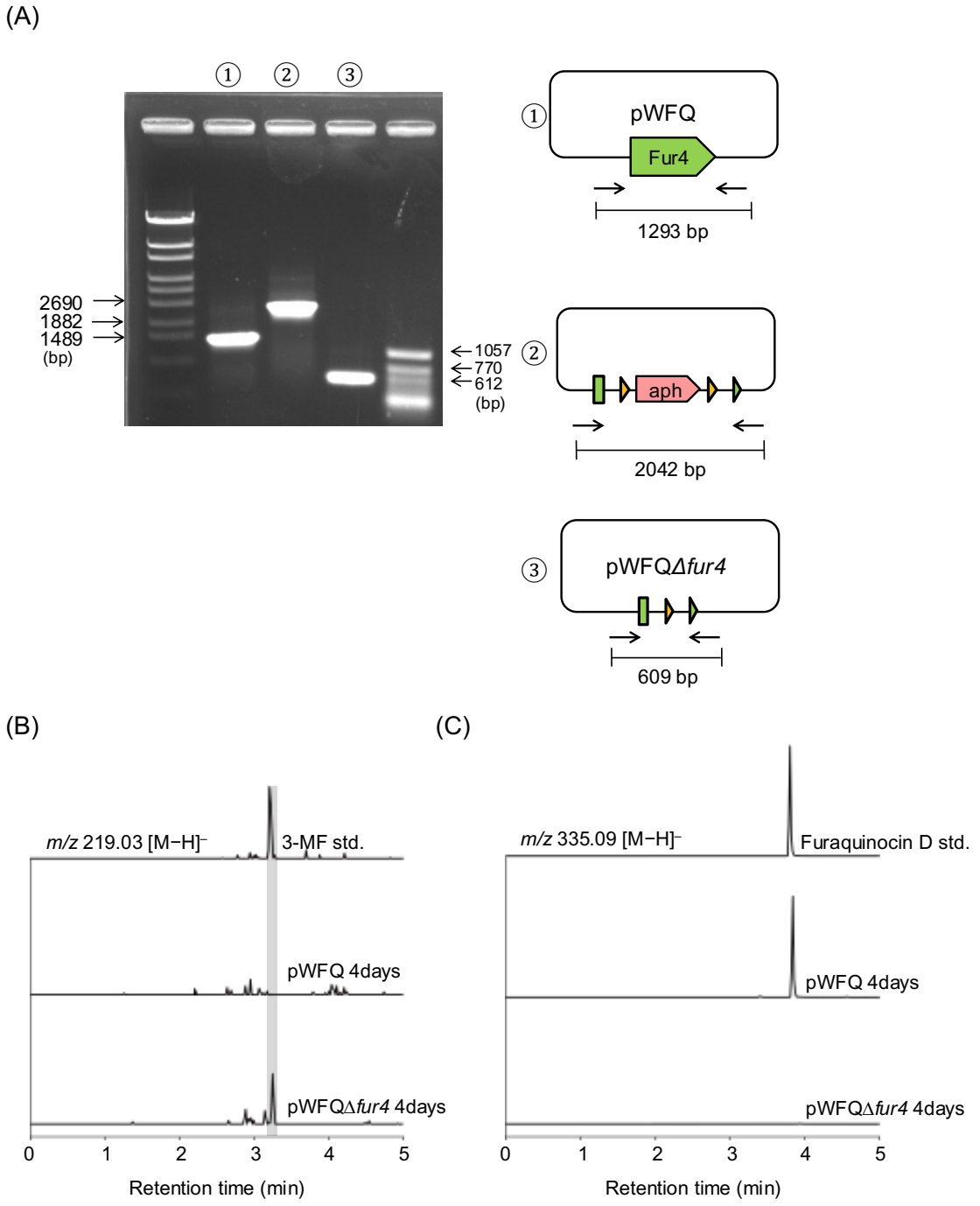

Figure S28. Gene disruption of *fur4* and heterologous expression analysis of pWFQΔ*fur4*.

(A) Gene disruption and confirmation of *fur4* gene on pWFQ vector. The *fur4* gene was disrupted in-frame, and disruption was confirmed by the amplified length of the region between the two primers d_fur4_check_f and d_fur4_check_r by PCR. (Table S2) **(B)(C)** Extracted ion chromatograms of culture medium of *S. albus* G153 transformed with pWFQ or pWFQΔ*fur4*. (**B:** 219.03 $[M-H]^-$ for 3-MF, **C**: 385.18 $[M-H]^-$ for Furaquinocin D).

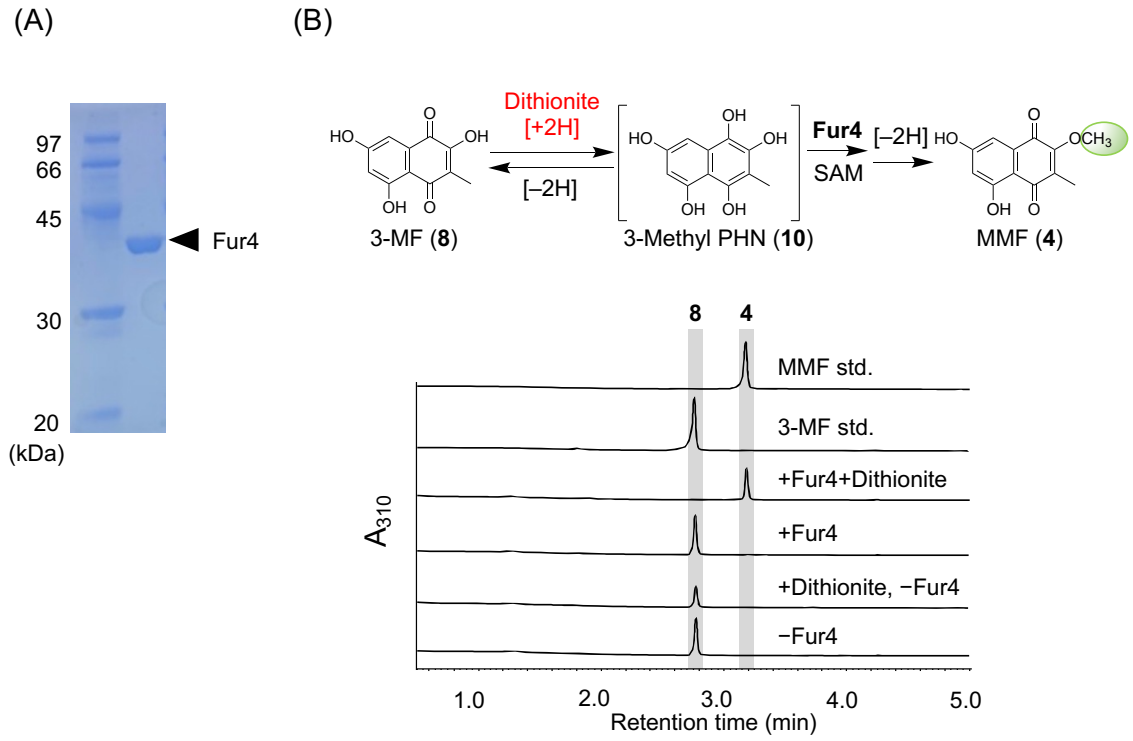

Figure S29. Methylation by Fur4.

(A) SDS–PAGE analysis of Fur4. The molecular weight of Fur4 is 37 kDa. **(B)** The LC–UV/VIS chromatograms of the Fur4 reaction mixture. A_{310}, absorbance at 310 nm. Methylation by Fur4 proceeded under reduced conditions, in which 3-MF (**8**) is reduced to 3-methyl PHN (**10**). The assay conditions are described in the Supporting Information.

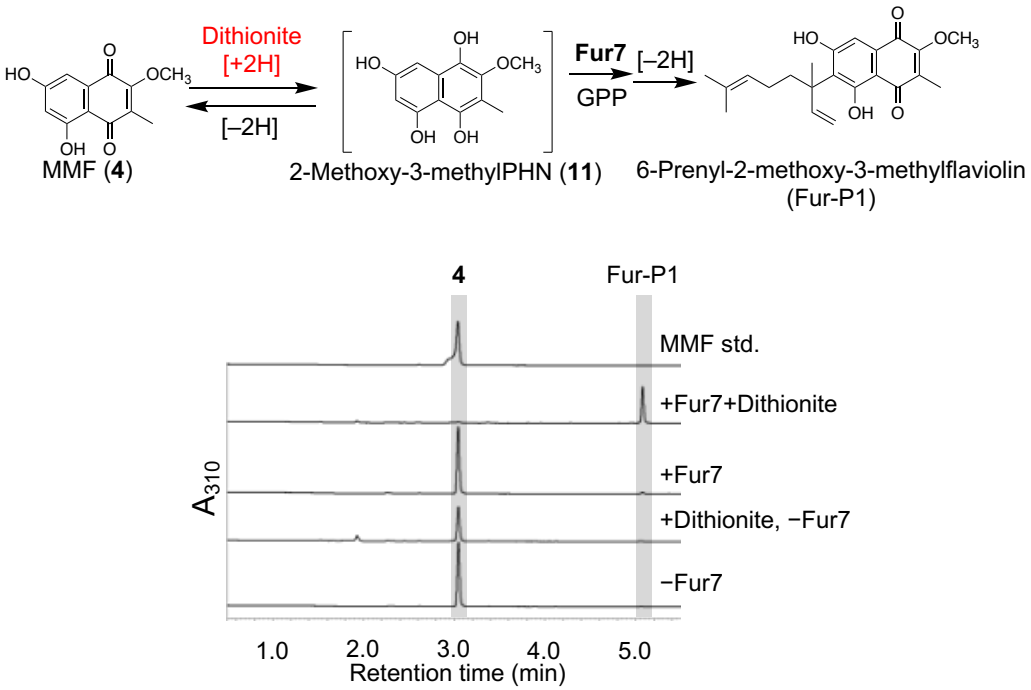

Figure S30. Geranylation by Fur7.

The LC–UV/VIS chromatograms of Fur7. A_{310}, absorbance at 310 nm. Geranylation by Fur7 proceeded in a reduced condition. The assay conditions are described in the Supporting Information. In the +Fur7+dithionite condition, the substrate MMF (**4**) was completely consumed and converted to Fur-P1. Fur-P1 was also detected in the +Fur7 condition but in very small amounts.

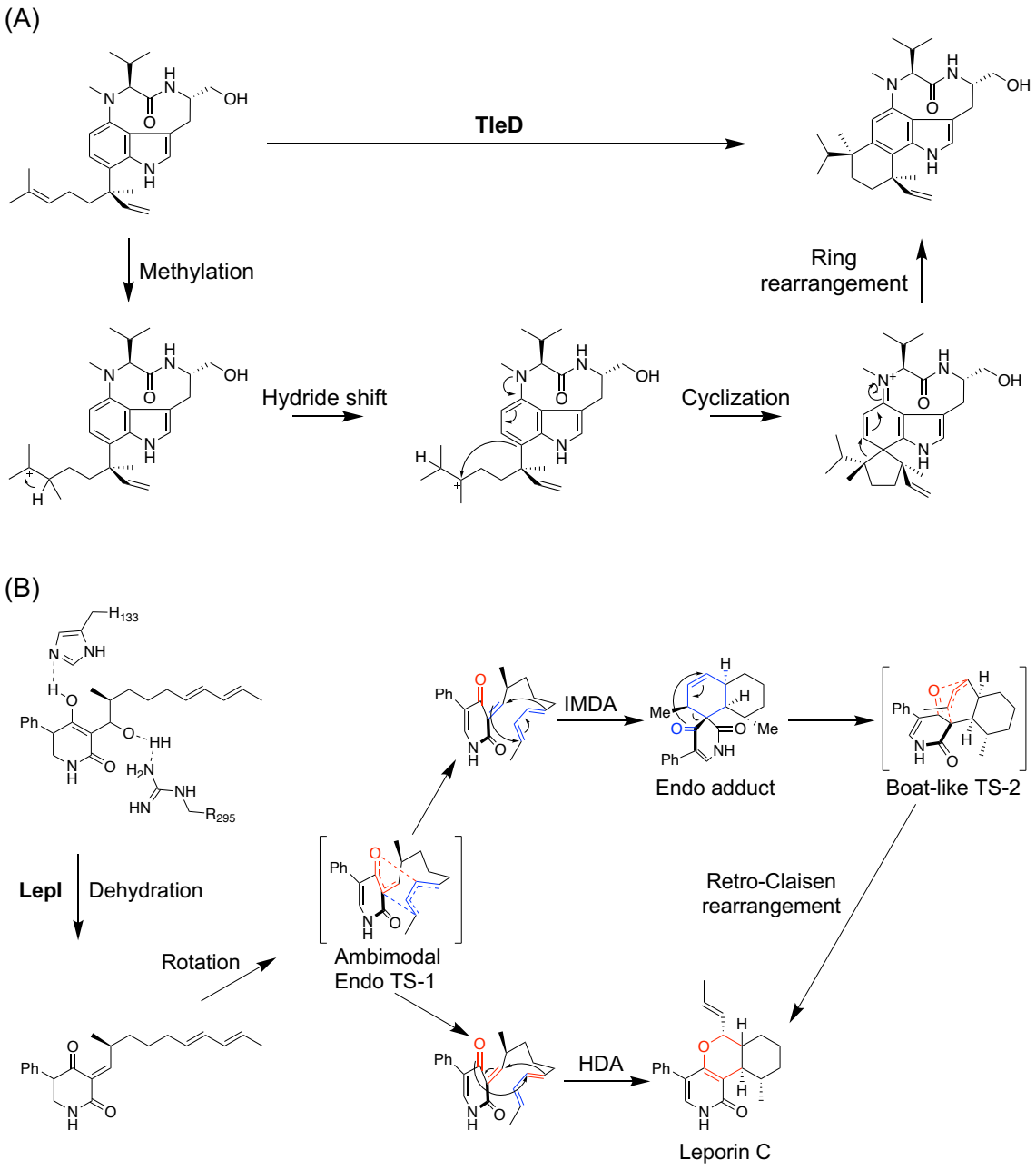
(A)
TleD
Methylation
Ring rearrangement
Hydride shift
Cyclization
(B)
LepI
Dehydration
Rotation
Ambimodal Endo TS-1
IMDA
Endo adduct
Boat-like TS-2
Retro-Claisen rearrangement
HDA
Leporin C

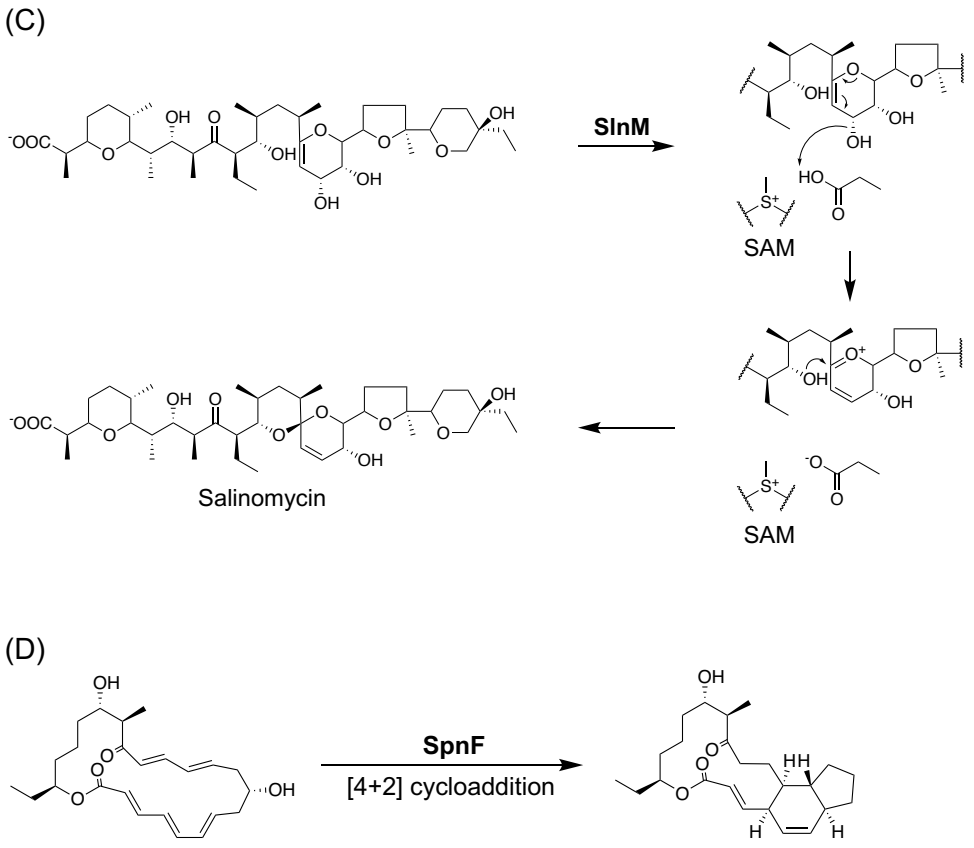

Figure S31. Reaction mechanism of cyclisation reactions catalyzed by SAM-dependent methyltransferase homologs.

(A) Cyclization reaction catalyzed by methyltransferase TleD. **(B)** Cyclization reaction catalyzed by methyltransferase homolog SlmM. **(C)** Intramolecular Diels-Alder (IMDA) and hetero-Diels-Alder (HAD) reactions catalyzed by methyltransferase-like LepI. **(D)** [4+2] cycloaddition reaction catalyzed by methyltransferase-like SpnF.

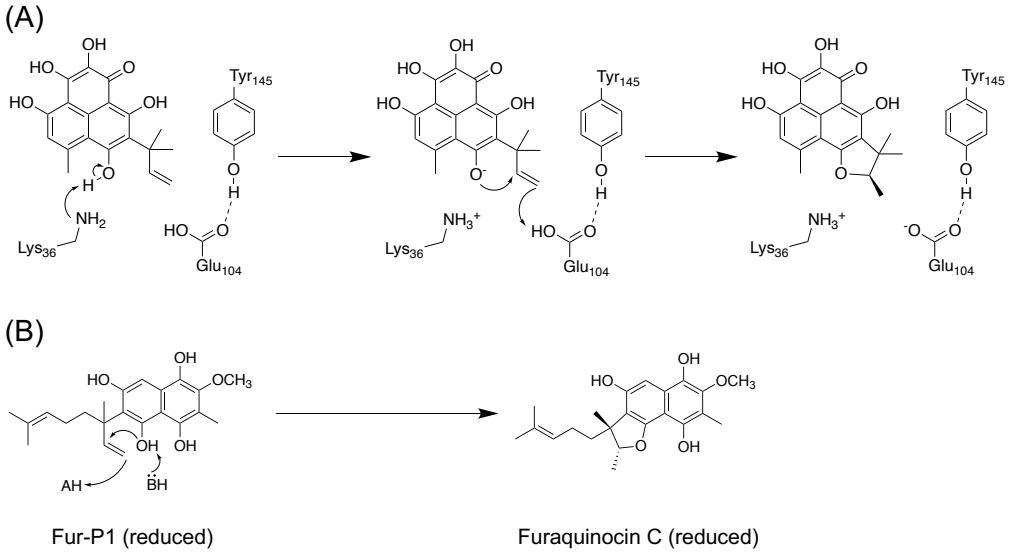

Figure S32. Hydroalkoxylation by enzymes.

(A) Proposed reaction mechanism of cyclization catalyzed by PhnH in the DUF3237 superfamily. **(B)** Proposed reaction mechanism of Fur21.

Supplementary References

[1] S. Isogai, M. Nishiyama, T. Kuzuyama, *Bioorg. Med. Chem. Lett.* **2012**, *22*, 5823–5826.
[2] T. Kumano, T. Tomita, M. Nishiyama, T. Kuzuyama, *J. Biol. Chem.* **2010**, *285*, 39663–39671.
[3] J. M. Jez, J. L. Ferrer, M. E. Bowman, R. A. Dixon, J. P. Noel, *Biochemistry* **2000**, *39*, 890–902.
[4] T. Dairi, K. Aisaka, R. Katsumata, M. Hasegawa, *Biosci. Biotechnol. Biochem.* **1995**, *59*, 1835–1841.
[5] T. Kawasaki, Y. Hayashi, T. Kuzuyama, K. Furihata, N. Itoh, H. Seto, T. Dairi, *J. Bacteriol.* **2006**, *188*, 1236–1244.
[6] Y. Hamano, C. Maruyama, H. Kimoto, *Nippon. Hosenkin Gakkaishi.* **2006**, *20*, 35–41.
[7] T. Kieser, *Practical Streptomyces Genetics*, John Innes Foundation, Norwich, **2000**.
[8] S. Kawai, A. Yamada, D. Du, Y. Sugai, Y. Katsuyama, Y. Ohnishi, *ACS Chem. Biol.* **2023**, *18*, 1821–1828.
[9] W. Kabsch, *Acta Crystallogr. D Biol. Crystallogr.* **2010**, *66*, 125–132.
[10] P. Skubák, N. S. Pannu, *Nat. Commun.* **2013**, *4*, 2777.
[11] A. J. McCoy, R. W. Grosse-Kunstleve, P. D. Adams, M. D. Winn, L. C. Storoni, R. J. Read, *J. Appl. Crystallogr.* **2007**, *40*, 658–674.
[12] M. D. Winn, C. C. Ballard, K. D. Cowtan, E. J. Dodson, P. Emsley, P. R. Evans, R. M. Keegan, E. B. Krissinel, A. G. W. Leslie, A. McCoy, S. J. McNicholas, G. N. Murshudov, N. S. Pannu, E. A. Potterton, H. R. Powell, R. J. Read, A. Vagin, K. S. Wilson, *Acta Crystallogr. D Biol. Crystallogr.* **2011**, *67*, 235–242.
[13] P. Emsley, B. Lohkamp, W. G. Scott, K. Cowtan, *Acta Crystallogr. D Biol. Crystallogr.* **2010**, *66*, 486–501.
[14] G. N. Murshudov, P. Skubák, A. A. Lebedev, N. S. Pannu, R. A. Steiner, R. A. Nicholls, Winn, F. Long, A. A. Vagin, *Acta Crystallogr. D Biol. Crystallogr.* **2011**, *67*, 355–367.
[15] C. J. Williams, J. J. Headd, N. W. Moriarty, M. G. Prisant, L. L. Videau, L. N. Deis, V. Verma, D. A. Keedy, B. J. Hintze, V. B. Chen, S. Jain, S. M. Lewis, W. B. Arendall 3rd, J. Snoeyink, P. D. Adams, S. C. Lovell, J. S. Richardson, D. C. Richardson, *Protein Sci.* **2018**, *27*, 293–315.
[16] J. R. Greenwood, D. Calkins, A. P. Sullivan, J. C. Shelley, *J. Comput. Aided Mol. Des.* **2010**, *24*, 591–604.
[17] J. C. Shelley, A. Cholleti, L. L. Frye, J. R. Greenwood, M. R. Timlin, M. Uchimaya, *J. Comput. Aided Mol. Des.* **2007**, *21*, 681–691.
[18] Frisch, M.J., Trucks, G.W., Schlegel, H.B., Scuseria, G.E., Robb, M.A., Cheeseman, J.R., G. Scalmani, V. Barone, G. A. Petersson, H. Nakatsuji, X. Li, M. Caricato, A. V. Marenich, Bloino, J., Janesko, B.G., Gomperts, R., Mennucci, B., Hratchian, H.P., Ortiz, J.V., Izmaylov, A.F., Sonnenberg, J.L., Williams-Young, D., Ding, F., Lipparini, F., Egidi, F., Goings, J., Peng, B., Petrone, A., Henderson, T., Ranasinghe, D., Zakrzewski, V.G., Gao, J., Rega, N., Zheng, G., Liang, W., Hada, M., Ehara, M., Toyota, K., Fukuda, R., Hasegawa, J., Ishida, M., Nakajima, T., Honda, Y., Kitao, O., Nakai, H., Vreven, T., Throssell, K., Montgomery Jr., J.A., Peralta, J.E., Ogliaro, F., Bearpark, M.J., Heyd, J.J., Brothers, E.N., Kudin, K.N., Staroverov, V.N., Keith, T.A., Kobayashi, R., Normand, J., Raghavachari, K., Rendell, A.P., Burant, J.C., Iyengar, S.S., Tomasi, J., Cossi, M., Millam, J.M., Klene, M., Adamo, C., Cammi, R., Ochterski, J.W., Martin, R.L., Morokuma, K., Farkas, O., Foresman, J.B., Fox, D.J., *Gaussian 16 Rev. B.01, Gaussian, Inc., Wallingford, CT*, **2016**.

[19] J. Wang, W. Wang, P. A. Kollman, D. A. Case, *J. Mol. Graph. Model.* **2006**, *25*, 247–260.
[20] J. A. Maier, C. Martinez, K. Kasavajhala, L. Wickstrom, K. E. Hauser, C. Simmerling, *J. Chem. Theory Comput.* **2015**, *11*, 3696–3713.
[21] D. L. Mobley, C. I. Bayly, M. D. Cooper, M. R. Shirts, K. A. Dill, *J. Chem. Theory Comput.* **2015**, *11*, 1347.
[22] D. A. Case, T. E. Cheatham 3rd, T. Darden, H. Gohlke, R. Luo, K. M. Merz Jr, A. Onufriev, C. Simmerling, B. Wang, R. J. Woods, *J. Comput. Chem.* **2005**, *26*, 1668–1688.
[23]W. L. Jorgensen, J. Chandrasekhar, J. D. Madura, R. W. Impey, M. L. Klein, *J. Chem. Phys.* **1983**, *79*, 926–935.
[24] T. Darden, D. York, L. Pedersen, *J. Chem. Phys.* **1993**, *98*, 10089–10092.
[25] J.-P. Ryckaert, G. Ciccotti, H. J. C. Berendsen, *J. Comput. Phys.* **1977**, *23*, 327–341.
[26] H. J. C. Berendsen, J. P. M. Postma, W. F. Van Gunsteren, A. Dinola, J. R. Haak, *J. Chem. Phys.* **1984**, *81*, 3684–3690.
[27] D.A. Case, K. Belfon, I.Y. Ben-Shalom, S.R. Brozell, D.S. Cerutti, T.E. Cheatham, III, V.W.D. Cruzeiro, T.A. Darden, R.E. Duke, G. Giambasu, M.K. Gilson, H. Gohlke, A.W. Goetz,R Harris, S. Izadi, S.A. Izmailov, K. Kasavajhala, A. Kovalenko, R. Krasny, T. Kurtzman, T.S. Lee, S. LeGrand, P. Li, C. Lin, J. Liu, T. Luchko, R. Luo, V. Man, K.M. Merz, Y. Miao, O. Mikhailovskii, G. Monard, H. Nguyen, A. Onufriev, F. Pan, S. Pantano, R. Qi, D.R. Roe, A. Roitberg, C. Sagui, S. Schott-Verdugo, J. Shen, C.L. Simmerling, N.R. Skrynnikov, J. Smith, J. Swails, R.C. Walker, J. Wang, L. Wilson, R.M. Wolf, X. Wu, Y. Xiong, Y. Xue, D.M. York and P.A. Kollman, *AMBER 2020, University of California, San Francisco*, **2020**.
[28] M. Komatsu, T. Uchiyama, S. Omura, D. E. Cane, H. Ikeda, **2010**, *107*, DOI 10.1073/pnas.0914833107.
[29] K. A. Datsenko, B. L. Wanner, *Proceedings of the National Academy of Sciences* **2000**, *97*, 6640–6645.